



Cite this: *Catal. Sci. Technol.*, 2015, 5, 2649

# Low temperature catalytic oxidation of volatile organic compounds: a review

Haibao Huang,<sup>\*a</sup> Ying Xu,<sup>a</sup> Qiuyu Feng<sup>a</sup> and Dennis Y. C. Leung<sup>\*b</sup>

Volatile organic compounds (VOCs) are toxic and recognized as one of the major contributors to air pollution. The development of efficient processes to reduce their emissions is highly required. Complete catalytic oxidation is a promising way to convert VOCs, especially with low concentration, into harmless CO<sub>2</sub> and water. This reaction is highly desirable to proceed at low temperature for the consideration of safety, energy savings, low cost and environmental friendliness. Great efforts have been devoted to develop efficient catalysts in order to reduce the temperature of catalytic oxidation of VOCs. The present review highlights recent important progress in the development of supported noble metal and metal oxide catalysts in this field. We examined several typical metals that are widely adopted as essential components for catalytic oxidation of VOCs and explored the effect of some important influencing factors such as the properties of metal and support, dispersion, particle size and morphology of metals. The specific mechanism that leads to superior catalytic activity towards low temperature VOC oxidation was discussed too.

Received 26th December 2014,  
Accepted 11th February 2015

DOI: 10.1039/c4cy01733a

www.rsc.org/catalysis

## 1. Introduction

Volatile organic compounds (VOCs) with boiling points between room temperature and 260 °C are recognized as the major contributors to global air pollution.<sup>1</sup> They are the precursors of ozone, photochemical smog and secondary aerosols, and many VOCs, such as benzene and toluene, are especially harmful to human beings due to their toxic, malodorous, mutagenic and carcinogenic nature.<sup>2–5</sup> In recent years, the extremely severe and persistent haze pollution frequently appeared in developing countries with rapid industrialization and urbanization, especially in China. Stringent controls for VOC emissions could be the kind of efficient measure needed to mitigate haze pollution.<sup>6</sup> By 2020, VOC emissions are predicted to increase by 49% relative to 2005 levels in China. The anthropogenic sources of VOCs include different human activities such as transportation and many factories or industrial processes including chemical, power and pharmaceutical plants, gas stations, petroleum refining, printing, shoemaking, food processing, automobile, furniture and textile manufacturing.<sup>7</sup> VOCs are also the most abundant and harmful chemical pollutants in indoor air.<sup>8</sup> Among the indoor sources, solvents, glue, insulating materials and

cooking and tobacco smoke are considered as the major contributors to VOC emission.<sup>1,9,10</sup>



Dennis Y. C. Leung

*Prof. Dennis Y. C. Leung received his BEng in 1982 and PhD in 1988, both from the Department of Mechanical Engineering at the University of Hong Kong. He had worked in Hongkong Electric Co., Ltd. for five years before joining the University of Hong Kong in 1993. Professor Leung is now a full professor in the Department of Mechanical Engineering specializing in air pollution control and renewable energy. He has published more*

*than 400 articles in this research area including 200 peer reviewed SCI journal papers with high impact factors. His h-index is 42 and total citations are more than 8000. He is one of the top 1% highly cited scientists in the world since 2010 (Essential Science Indicators) until now. He serves as a chief editor or editorial board member of many journals including Frontiers in Environmental Sciences, Applied Energy, Journal of Global Environment, Journal of Power & Energy, Chinese Science Bulletin, Sustainable Energy, etc. Prof. Leung received numerous awards including the Outstanding Earth Champion Hong Kong award in 2008 for recognizing his contributions in protecting the environment.*

<sup>a</sup> School of Environmental Science and Engineering, Sun Yat-Sen University, Guangzhou 510275, China. E-mail: seabao8@gmail.com

<sup>b</sup> Department of Mechanical Engineering, The University of Hong Kong, Pokfulam Road, Hong Kong. E-mail: ycleung@hku.hk

The impact of VOCs on the environment depends on the nature of VOCs and their emission processes. Among the most common and toxic non-halogenated compounds, benzene, toluene, formaldehyde, propylene, phenol, acetone, and styrene cause the major concern for scientists.<sup>1</sup> Formaldehyde, which is an important chemical widely used by industry to manufacture building materials and household products, has the probability to cause cancer in animals and humans.<sup>11</sup> Aromatics and alkenes, the major families of pollutants in industrial and automotive emissions, particularly propylene and toluene are well recognized as highly polluting molecules because of their high Photochemical Ozone Creativity Potential (POCP).<sup>12,13</sup> Halogenated and other chlorinated VOCs such as dichloromethane, chloroform, carbon tetrachloride, 1,2-dichloroethane and trichloroethylene require special attention during their widespread applications in industry due to their high toxicity and stability.<sup>14</sup>

Because of their extremely harmful impact on the environment and the health of human beings as well as the tremendous growth in the amount of VOCs emitted, the release of VOCs into the environment is strictly being controlled in order to meet the increasingly stringent emission regulations worldwide. According to the Goteborg protocol, the maximum VOC emission level by 2020 in the European Union member countries should be reduced by nearly half as compared to the base year of 2000.<sup>15</sup> Therefore, the development of effective methods and materials for the abatement of VOCs is of great significance. Among those conventional control processes (e.g., incineration, condensation, biological degradation,<sup>16</sup> adsorption,<sup>17</sup> absorption, etc.) and emerging technologies (e.g., plasma catalysis,<sup>18</sup> photocatalytic oxidation,<sup>19,20</sup> ozone-catalytic oxidation,<sup>21</sup> etc.) for VOC abatement,<sup>22,23</sup> catalytic oxidation is considered to be the most promising method for VOC destruction.<sup>22,24,25</sup> Unlike adsorption, in which VOCs are just transferred from gas phase to adsorbent and the adsorbent needs frequent regeneration, catalytic oxidation can destroy VOCs and convert them into harmless

CO<sub>2</sub> and water.<sup>26</sup> Thermal incineration is a convenient approach to convert VOCs into carbon dioxide and water. However, it demands a high temperature operation and wastes a large amount of energy. Lots of toxic by-products are generated from VOC incineration. In contrast, catalytic oxidation can be operated at a lower temperature, and the selectivity of catalytic oxidation could be controlled as well.

However, some problems remain to be solved with VOC catalytic oxidation. In contrast to other industrial catalytic oxidation reactions, complete catalytic oxidation of VOCs in air is carried out at lower reactant concentrations (often less than 1000 ppm) and with a very large stoichiometric excess of oxygen. Although VOC oxidation is an exothermic reaction, the whole process consumes energy and is expensive when the reactant concentration is low since the entire gas stream must be heated to an elevated temperature,<sup>25</sup> generally much higher than 200 °C.<sup>27–29</sup> It has the risk of explosion and the formation of NO<sub>x</sub> by-products for heating the entire gas stream to a high temperature.<sup>25,30</sup> In addition, the catalysts tend to sinter more easily in a high temperature atmosphere. Therefore, catalytic oxidation of VOCs is highly desirable to proceed at low temperature, preferably at ambient temperature, for the consideration of safety, energy savings, low cost and environmental friendliness. Furthermore, the practical reaction environments are usually very complicated,<sup>31</sup> and the trace pollutants in air streams may include water vapor, ammonia, organohalogens and sulfur-containing compounds. These trace contaminants are, by general rule, poisons for industrial oxidation catalysts such as supported Pt or Ni.<sup>32,33</sup> Therefore, highly active, nonselective and stable catalysts are generally required to achieve catalytic oxidation of VOCs at low temperature.<sup>15,25</sup>

In recent years, great efforts have been devoted to develop efficient catalysts for the purpose of reducing the temperature of catalytic oxidation of VOCs. Generally, there are two major types of efficient catalysts developed for total VOC oxidation and they are supported noble metals and transition metal oxides. Owing to the unremitting efforts after so many years, highly efficient catalysts have been successfully developed for catalytic oxidation of VOC at low temperatures, even at room temperature in some cases.<sup>34,35</sup>

In this review, we mainly focus on the progress in complete catalytic oxidation of VOCs operated at low temperature (generally below 200 °C) or even at room temperature. Principally, the review will be divided into three parts. We started with a brief description of the general reaction mechanism in the first section. The second and third sections deal with catalytic oxidation of VOCs over supported noble metals and transition metal oxides, respectively. In both cases, we examined several typical metals that are widely studied as the essential components for catalytic oxidation of VOCs and explored the effect of some important influencing factors such as the properties of metals and their support, dispersion, particle size and morphology of metals. The specific mechanism which leads to the superior catalytic activity towards low temperature VOC oxidation was discussed.



**Haibao Huang**

*Haibao Huang was born in 1979 in Ganzhou, China. He received his BSc (2001) and PhD (2008) degree in Engineering from South China University of Technology. He joined Tsinghua University in 2008 and then moved to the University of Hong Kong in 2009 as a Post-doctoral Fellow and Senior Research Associate till 2012. He was a visiting Scholar at the University of Adelaide, Australia, from June to August, 2011. Since*

*2012, he has served as an associate professor in Sun Yat-Sen University in China. His research interest includes VOC control and environmental catalysis.*

Finally, we present some challenges of low temperature catalytic oxidation of VOCs and our perspectives on the future development in this field.

## 2. General reaction mechanism

Although low temperature catalytic oxidation of CO was intensively studied and the mechanism has been well addressed, it is still difficult to extend the results obtained from this reaction to catalytic oxidation of VOCs due to the different properties of pollutants and reaction conditions.<sup>25</sup> As a matter of fact, a general mechanism for complete oxidation of VOCs has not come into agreement until now.

The mechanism proposed for a complete catalytic oxidation of VOCs generally consists of three trends. It has been explained by the Mars–van Krevelen (MVK) model, as proposed by Kroger in 1932 and verified by Mars and van Krevelen in 1954.<sup>36–39</sup> This model assumes that the reaction will not be triggered until the organic molecules interact with the oxygen-rich parts on the surface of the catalyst. There are in general two successive steps in terms of the cyclic reaction. In the first step, oxygen vacancies on the catalyst surface were reduced as they react with the organic molecules. In the second step, the pre-formed reduced site regenerated immediately through the consumption of gaseous oxygen or the transfer of oxygen atoms from the bulk to the surface. Since the catalyst is reduced in the first step and then reoxidized in the second step, this mechanism is also known as the redox mechanism.

According to the combination method between oxygen molecules and pollutants, the reaction mechanism can be further divided into two mechanisms:<sup>15,40</sup> (1) Langmuir–Hinshelwood (L–H) mechanism, in which the reaction occurs between the adsorbed oxygen species and the adsorbed reactants. The controlling step is the surface reaction between two adsorbed molecules at analogous active sites; (2) Eley–Rideal (E–R) mechanism, in which the reaction proceeds between adsorbed oxygen species and reactant molecules in the gas phase. The controlling step is the reaction between an adsorbed molecule and a molecule from the gas phase.

The validity of each mechanism strongly depends on the properties of the catalyst (active metal and the support) as well as on the character of VOC molecules and it is really difficult to generalize. For example, the validity of the L–H mechanism for oxidation of olefins and aromatics over Pt/ $\gamma$ - $\text{Al}_2\text{O}_3$  catalysts is supported by the nature of the noble metal which is capable of electron transfer from the aromatic ring to the unoccupied d-orbitals as well as back-donation from the metal to the  $\pi^*$ -hydrocarbon orbitals. Accordingly, the L–H mechanism was proposed for oxidation of benzene, toluene, propene and 1-hexene.<sup>15</sup>

## 3. Supported noble metal catalysts

In spite of the expensive cost, noble metal based catalysts are recognized as the preferred ones for VOC catalytic oxidation because of their high specific activity, strong resistance to

deactivation and ability to be regenerated.<sup>40</sup> Platinum, gold, palladium, and silver are the most extensively studied elements of all the noble metals. They are generally supported by transition metal oxides such as  $\text{Al}_2\text{O}_3$ ,  $\text{TiO}_2$ ,  $\text{SiO}_2$ ,  $\text{MnO}_x$ ,  $\text{CeO}_2$ , and  $\text{Co}_3\text{O}_4$  and their mixtures increase the dispersion of noble metals and adsorption of reactants and also reduce the loading of noble metals. The catalytic performance of supported noble metals strongly depends on the metal's intrinsic properties, preparation method, precursors, support, the size and morphology of particles, *etc.*

The literature of the main data on catalytic oxidation of VOCs at low temperature over supported noble metal catalysts discussed in this review is summarized in Table 1.

### 3.1. Pt-based catalysts

Pt-based catalysts have always played a dominant role in industry due to their outstanding catalytic performance and they remain attractive for catalytic oxidation of VOCs.

The properties of the support, such as specific surface area, pore structure, acidity, surface hydrophobicity *etc.*, are critical to metal dispersion, VOC adsorption and metal–support interaction. They have been intensively investigated due to their great effect on catalytic activity. Among the supports,  $\gamma$ - $\text{Al}_2\text{O}_3$  was mostly studied and applied for catalytic oxidation of VOCs due to its large surface area, stability and low cost. Ordó *et al.*<sup>41</sup> used a commercial Pt/ $\gamma$ - $\text{Al}_2\text{O}_3$  catalyst for the catalytic oxidation of benzene, toluene and *n*-hexane in air, both alone and in binary mixtures. The temperatures for complete oxidation of these VOCs are all below 200 °C. Generally, the increased acid strength of the support is favorable for catalytic oxidation activity over supported Pt catalysts. Yazawa *et al.*<sup>42</sup> investigated the low temperature oxidation of propane over a supported platinum catalyst with a series of metal oxide supports such as MgO,  $\text{La}_2\text{O}_3$ ,  $\text{ZrO}_2$ ,  $\text{Al}_2\text{O}_3$ ,  $\text{SiO}_2$ ,  $\text{SiO}_2$ - $\text{Al}_2\text{O}_3$ , and  $\text{SO}_4^{2-}$ - $\text{ZrO}_2$ . Results indicated that platinum supported on materials with stronger acidity showed higher catalytic activity.

The particle sizes of noble metals are often regarded as an important parameter in supported noble metal catalysts. The turnover frequencies (TOFs) of HCHO oxidation over Pt nanoparticles presented a significant size-dependent effect.<sup>43</sup> They were nearly linearly increased with Pt nanoparticles and reached the highest value of 4.39  $\text{s}^{-1}$  over the Pt nanoparticles with an average size of 10.1 nm. As the particle size increases, the number of Pt atoms on (100) and (111) crystal facets increases with respect to those at the edges and corners too and the (100) and (111) crystal facets of Pt nanoparticles provide the appropriate sites for the reaction. The interface which is mainly determined by the size of Pt nanoparticles plays an essential role in achieving the high reactivity. It was also reported by Kim<sup>44</sup> that the strength of the surface Pt–O bond decreases when the Pt particle size is increased. The reactivity of adsorbed oxygen on the large Pt particles is higher than the reactivity on the small ones. As a consequence, the activation energy is much lower on the

**Table 1** Survey of literature data on catalytic oxidation of VOCs over noble metals at low temperature<sup>a</sup>

Catalysts	Preparation method	VOC type	Reaction mixture	$T_{90\%}$ , °C	Ref.
Pt/MCM-41	IM	Toluene Benzene Cumene Ethylbenzene Mesitylene	4340 to 45 000 ppm	150 220 250 300 350	40
Pt/Al <sub>2</sub> O <sub>3</sub>	Commercial	Benzene Toluene <i>n</i> -Hexane	4200 ppm Air balance	165 160–190 190–230	41
Pt on MgO, La <sub>2</sub> O <sub>3</sub> , ZrO <sub>2</sub> , Al <sub>2</sub> O <sub>3</sub> , SiO <sub>2</sub> , SiO <sub>2</sub> –Al <sub>2</sub> O <sub>3</sub> , Pt/SO <sub>4</sub> <sup>2–</sup> –ZrO <sub>2</sub>	IM	Propane	0.25% propane 1.25% O <sub>2</sub> N <sub>2</sub> balance	<327 <200	42
Pt/TiO <sub>2</sub>	IM	HCHO	40 ppm Air balance	RT	43
Pt–Au/ZnO/Al <sub>2</sub> O <sub>3</sub>	IMP	Toluene	1.8 mol% toluene Air balance	<200	44
Pt/Ce <sub>0.64</sub> Zr <sub>0.15</sub> Bi <sub>0.21</sub> O <sub>1.895</sub> /γ–Al <sub>2</sub> O <sub>3</sub>	IM	Toluene	900 ppm toluene Air balance	120	51
Pt/TiO <sub>2</sub> Rh/TiO <sub>2</sub> Pd/TiO <sub>2</sub> Au/TiO <sub>2</sub> Pt/TiO <sub>2</sub> Pt/SiO <sub>2</sub> Pt/Ce <sub>0.8</sub> Zr <sub>0.2</sub> O <sub>2</sub> Pt/Ce <sub>0.2</sub> Zr <sub>0.8</sub> O <sub>2</sub> Pt/TiO <sub>2</sub>	IM	HCHO	100 ppm HCHO 20% O <sub>2</sub> , He balance	RT	34, 53 and 54
	IM	HCHO	100 ppm HCHO 22% O <sub>2</sub> , N <sub>2</sub> balance	90 120 >120 >120	55
	IM	HCHO	10 ppm HCHO 50% H <sub>2</sub> O vapor, air balance	RT	35 and 57
Na/Pt/TiO <sub>2</sub>	IM	HCHO	600 ppm HCHO 20% O <sub>2</sub> , He balance, 50% H <sub>2</sub> O vapor	RT	58
Pt/Fe <sub>2</sub> O <sub>3</sub>	IM	HCHO	100–500 ppm HCHO 20% O <sub>2</sub> , N <sub>2</sub> balance	RT	60
Pt/MnO <sub>2</sub>	IM	HCHO	460 ppm HCHO Air balance	80	62
Pt/MnO <sub>x</sub> –CeO <sub>2</sub>	IM	HCHO	580 ppm HCHO 20% O <sub>2</sub> , He balance	RT	63
Pd/TiO <sub>2</sub> Pt/TiO <sub>2</sub> , Au/TiO <sub>2</sub> , Ag/TiO <sub>2</sub> , Rh/TiO <sub>2</sub> Pd/MgO, Al <sub>2</sub> O <sub>3</sub> , SiO <sub>2</sub> , SnO <sub>2</sub> , Nb <sub>2</sub> O <sub>5</sub> , WO <sub>3</sub> , ZrO <sub>2</sub>	IM	<i>o</i> -Xylene	100 ppm <i>o</i> -xylene 20% O <sub>2</sub> , N <sub>2</sub> balance	140 >140	70
	IM	Toluene	0.95% toluene Air balance	277	73
Pd/Co <sub>3</sub> AlO	CP	Toluene	0.08 vol.% toluene Air balance	230	74
Pd/BEA zeolites Pd/FAU zeolites	IM	Propene Toluene	6000 ppm propene 1000 ppm toluene Air balance	200 180 170 175	75
Pd/macro–mesoporous ZrO <sub>2</sub> Pd/macro–mesoporous TiO <sub>2</sub> Pd/macro–mesoporous ZrO <sub>2</sub> –TiO <sub>2</sub> Pd–Mn/Al <sub>2</sub> O <sub>3</sub>	IM	Toluene	1000 ppm toluene Air balance	280 150 240	77
	IM	Formaldehyde/methanol	0.53% HCHO 0.19% methanol 0.66% water, 22.98% O <sub>2</sub> , N <sub>2</sub> balance	<230	72
Pd/TiO <sub>2</sub>	IM DP	HCHO	10 ppm HCHO Air balance, 50% H <sub>2</sub> O vapor	RT	84
Na–Pd/TiO <sub>2</sub>	CP	HCHO	140 ppm HCHO 20% O <sub>2</sub> , 25% water vapor He balance	RT	86
Au/MnO <sub>2</sub>	DP	<i>n</i> -Hexane	125 ppm <i>n</i> -hexane 20% O <sub>2</sub> , N <sub>2</sub> balance	180	99
Au/Fe <sub>2</sub> O <sub>3</sub>	CP	Methanol 2-Propanol Toluene	0.7% VOCs 10% O <sub>2</sub> , He balance	<200 <200 310	96
Au/Fe <sub>2</sub> O <sub>3</sub>	CP	Methanol Ethanol 2-Propanol	0.7% VOCs 10% O <sub>2</sub> , He balance	<200 <200 <200	100



Table 1 (continued)

Catalysts	Preparation method	VOC type	Reaction mixture	$T_{90\%}$ , °C	Ref.
Au/CoO <sub>x</sub>	CP	Acetone		<300	
Au/MnO <sub>x</sub>	DP	Toluene		<400	
Au/CuO	IM	CH <sub>4</sub>	0.5%	<200	101
Au/Fe <sub>2</sub> O <sub>3</sub>		C <sub>2</sub> H <sub>6</sub>	Air balance	<400	
Au/CeO <sub>2</sub>		C <sub>3</sub> H <sub>8</sub>		<400	
Au/CoO <sub>x</sub>	DP	C <sub>3</sub> H <sub>8</sub>	8000 ppm	200	102
Au/CeO <sub>2</sub> /Al <sub>2</sub> O <sub>3</sub> Au/Al <sub>2</sub> O <sub>3</sub>	DP	Toluene	Air balance		
		<i>n</i> -Hexane	120 ppm	<350	103
		Benzene	250 ppm	<300	
		2-Propanol	500 ppm	<250	
Au/CeO <sub>2</sub>	CP	Methanol	0.7% VOCs	<200	104
	DP	2-Propanol	10% O <sub>2</sub> , He balance	<200	
		Toluene		<300	
Au/TiO <sub>2</sub>	DP	C <sub>3</sub> H <sub>8</sub>	1000 ppm	<200	105
Au/CeO <sub>2</sub>		Toluene	9% O <sub>2</sub> , He balance	<250	
Au/Al <sub>2</sub> O <sub>3</sub>					
Au/CeO <sub>2</sub> -Al <sub>2</sub> O <sub>3</sub>					
Au/TiO <sub>2</sub>	CP	HCHO	—	80	107
Au/CeO <sub>2</sub>					
Au/TiO <sub>2</sub> -CeO <sub>2</sub>	CP	HCHO	0.06% HCHO	<100	108
Au/CeO <sub>2</sub>			Air balance		
Au/CeO <sub>2</sub>	DP	HCHO	500 ppm HCHO	37	109
			20% O <sub>2</sub> , N <sub>2</sub> balanced		
Au/Fe-O	CP	HCHO	6.25 ppm HCHO	<80	110
			Air balance		
Au/ZrO <sub>2</sub>	DP	HCHO	90 ppm HCHO	<200	112
			Air balance		
3DOM Au/CeO <sub>2</sub>	DP	HCHO	0.06% HCHO	<40	113
			Air balance		
3DOM Au/CeO <sub>2</sub> -Co <sub>3</sub> O <sub>4</sub>	DP	HCHO	0.06% HCHO	<80	114
			Air balance		
3DOM Au/Co <sub>3</sub> O <sub>4</sub>	CDP	Benzene	1000 ppm VOC	<200	117
		Toluene	VOC/O <sub>2</sub> = 1/400	<150	
		<i>o</i> -Xylene	N <sub>2</sub> balance	<150	
Ag/CeO <sub>2</sub>	CP	HCHO	0.42% HCHO	<150	121
			0.074% CH <sub>3</sub> OH		
Ag <sub>2</sub> O/CeO <sub>2</sub>			19.9% H <sub>2</sub> O, 62.7% N <sub>2</sub> , 16.9% O <sub>2</sub>		
Ag/SiO <sub>2</sub>	IMP	HCHO	1.8% HCHO	<200	122
Ag/Al <sub>2</sub> O <sub>3</sub>			14.8% O <sub>2</sub> , He balance		
Ag/SBA-15	IMP	HCHO	1000 ppm	<100	124
	Post-grafting method		15% O <sub>2</sub> , He balance		
Ag/MnO <sub>x</sub> -CeO <sub>2</sub>	DP	HCHO	580 ppm	<100	125
			18% O <sub>2</sub> , He balance		
3DOM Ag/Co <sub>3</sub> O <sub>4</sub>	IMP	HCHO	100 ppm	<80	126
			20% O <sub>2</sub> , N <sub>2</sub> balance		
Ag/hollandite	Thermal processing	HCHO	400 ppm	<100	127
			10% O <sub>2</sub> , N <sub>2</sub> balance		

<sup>a</sup> IMP: impregnation, DP: deposition-precipitation, CP: co-precipitation, CDP: colloidal deposition, RT: room temperature.

large Pt particles, due to the easy adsorption and desorption of oxygen and, therefore, their catalytic activity is higher. Similar results have been reported for the complete oxidation of propene and toluene over Pt/ $\gamma$ -Al<sub>2</sub>O<sub>3</sub> by Garetto *et al.*<sup>45</sup> A series of Pt/ $\gamma$ -Al<sub>2</sub>O<sub>3</sub> with different specific surface areas and Pt dispersions were prepared using different  $\gamma$ -Al<sub>2</sub>O<sub>3</sub> supports and Pt precursors. Catalytic activities for propene combustion are similar and irrespective of the specific surface areas and

pore sizes of  $\gamma$ -Al<sub>2</sub>O<sub>3</sub> supports. The loading and the size of the metallic particles of Pt have a great influence on catalytic performance during the complete oxidation of propene and toluene. Complete oxidation of VOCs is favored by an increased Pt content which increased the number of active sites. Propene intrinsic catalytic activities, expressed in mol<sub>VOC</sub> s<sup>-1</sup> g<sub>Pt</sub><sup>-1</sup>, were increased with an increase in particle size within the range of 1–3 nm. This could be attributed to

the strength of the Pt–O bond, which is weaker for larger particles and forms more reactive adsorbed oxygen species. However, the decreased activity is expected for larger particle sizes, of which Pt surface area is too small.<sup>43</sup>

It was reported that porous multimodal oxide materials as noble metal catalyst supports offered not only a higher activity in VOC oxidation but also better reaction conditions that could avoid the formation of by-products and the deposition of coke on the catalysts.<sup>46</sup> They provide a large surface area for the dispersion of noble metal. Compared with Pt/ $\gamma$ -Al<sub>2</sub>O<sub>3</sub>, molecular sieve supported Pt catalysts like Pt/H-ZSM-5 and Pt/MCM-41 showed better activity towards catalytic oxidation of aromatics.<sup>47,48</sup> However, water vapor generated from VOC oxidation or in gas flow can be easily condensed in the micro/mesopores due to hydrophilicity at low temperature, which results in catalytic deactivation. However, hydrophobic catalysts can avoid such a problem. Thus, the active sites would not be cloaked and catalytic activities could be maintained, especially at low temperature.<sup>49</sup> Various hydrophobic supports such as polystyrene–divinylbenzene (SDB), activated carbon,<sup>49</sup> activated carbon fibers<sup>50</sup> and carbon aerogels<sup>9</sup> were used to prepare Pt catalysts for VOC oxidation and they exhibited superior catalytic activities for BTX oxidation. Hydrophobic Pt/SDB showed the highest activity among the prepared catalysts and could completely oxidize toluene at temperature as low as 150 °C.<sup>49</sup> It was suggested that the rate of toluene oxidation might be enhanced due to the fact that water, one of the products, was expelled from the hydrophobic surface.

Many efforts were further made to develop efficient Pt catalysts for VOC oxidation at lower temperatures. Recently, Toshiyuki Masui *et al.*<sup>51</sup> reported that a complete oxidation of toluene was achieved at a temperature as low as 120 °C on a 7%Pt/16%Ce<sub>0.64</sub>Zr<sub>0.15</sub>Bi<sub>0.21</sub>O<sub>1.895</sub>/ $\gamma$ -Al<sub>2</sub>O<sub>3</sub> catalyst (Fig. 1). In

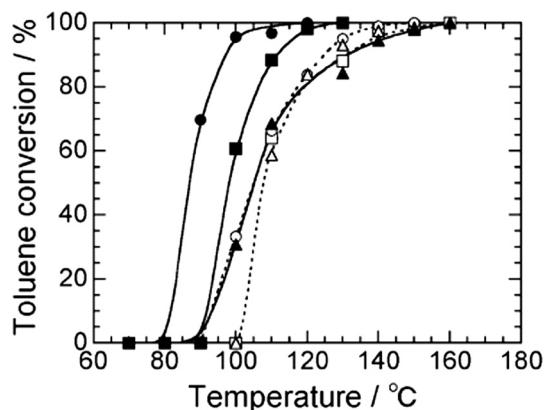


Fig. 1 Temperature dependence of the toluene oxidation on 5% Pt/CZB/Al<sub>2</sub>O<sub>3</sub> (□, ■), 7% Pt/CZB/Al<sub>2</sub>O<sub>3</sub> (○, ●), and 9% Pt/CZB/Al<sub>2</sub>O<sub>3</sub> (△, ▲) prepared without PVP. Open and closed symbols correspond to the data for the samples prepared in the absence and presence of PVP, respectively.<sup>51</sup> (Reprinted with permission from T. Masui, H. Imadzu, N. Matsuyama and N. Imanaka, Total oxidation of toluene on Pt/CeO<sub>2</sub>–ZrO<sub>2</sub>–Bi<sub>2</sub>O<sub>3</sub>/ $\gamma$ -Al<sub>2</sub>O<sub>3</sub> catalysts prepared in the presence of polyvinyl pyrrolidone, *J. Hazard. Mater.*, 2010, **176**, 1106–1109. Copyright 2010, Elsevier).

the previous studies,<sup>52</sup> the same authors found that a Ce<sub>0.64</sub>Zr<sub>0.16</sub>Bi<sub>0.20</sub>O<sub>1.90</sub>/ $\gamma$ -Al<sub>2</sub>O<sub>3</sub> solid can supply reactive oxygen molecules below 100 °C. With the addition of platinum, the mobility of the lattice oxygen increased in the near surface region of the catalyst, resulting in the accelerated reaction rate.

Recently, Zhang and He *et al.*<sup>34,53,54</sup> made a breakthrough in developing highly efficient catalysts for the total oxidation of formaldehyde (HCHO) at room temperature. They prepared a 1 wt.% Pt/TiO<sub>2</sub> catalyst by a simple impregnation method. HCHO can be completely oxidized into CO<sub>2</sub> and H<sub>2</sub>O over the Pt/TiO<sub>2</sub> catalyst at room temperature without any by-products, indicating that TiO<sub>2</sub> is a favorable support for HCHO catalytic oxidation at room temperature. They continued their research by comparing the performance of various noble metals supported on TiO<sub>2</sub> for catalytic oxidation of HCHO. It was found that the activity sequence was as follows: Pt/TiO<sub>2</sub> ≫ Rh/TiO<sub>2</sub> > Pd/TiO<sub>2</sub> > Au/TiO<sub>2</sub> ≫ TiO<sub>2</sub>. As shown in Fig. 2, it is evident that Pt/TiO<sub>2</sub> achieved a 100% HCHO removal while the other three catalysts were much less effective under the same reaction conditions. A simplified reaction mechanism for HCHO catalytic oxidation over TiO<sub>2</sub> supported noble metals was proposed by *in situ* DRIFTS. It is indicated that surface formate and CO species are the main reaction intermediates during the HCHO oxidation and the different activities of the noble metals were closely related to their capability to form formate species and to decompose formate into CO, which is the rate determining step for HCHO catalytic oxidation.

Peng and Wang<sup>55</sup> also studied catalytic activities of a series of metals (Pt, Pd, Rh, Cu, Mn) supported on TiO<sub>2</sub> and found that Pt/TiO<sub>2</sub> exhibited the best activity for the HCHO oxidation, which is similar to the results reported by Zhang.<sup>53</sup>

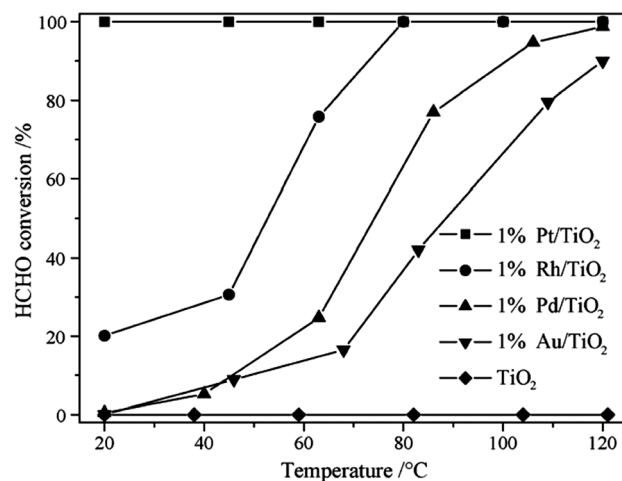


Fig. 2 HCHO conversions over TiO<sub>2</sub> (◆), Pt/TiO<sub>2</sub> (■), Rh/TiO<sub>2</sub> (●), Pd/TiO<sub>2</sub> (▲), and Au/TiO<sub>2</sub> (▼) catalysts at various temperatures. Reaction conditions: HCHO 100 ppm, O<sub>2</sub> 20 vol.%, He balance, total flow rate: 50 cm<sup>3</sup> min<sup>−1</sup>, GHSVs 50 000 h<sup>−1</sup>.<sup>53</sup> (Reprinted with permission from C. Zhang and H. He, A comparative study of TiO<sub>2</sub> supported noble metal catalysts for the oxidation of formaldehyde at room temperature, *Catal. Today*, 2007, **126**, 345–350. Copyright 2007, Elsevier).

In addition, they investigated the effect of the supports and found that the activity sequence of 0.6 wt.% Pt in various supports is  $\text{TiO}_2 > \text{SiO}_2 > \text{Ce}_{0.8}\text{Zr}_{0.2}\text{O}_2 > \text{Ce}_{0.2}\text{Zr}_{0.8}\text{O}_2$ . The catalytic activity was closely correlated with the dispersion of platinum on supports rather than the specific surface areas of supports. The higher dispersion of platinum can provide a larger number of catalytic sites.

Although supported Pt catalysts have been proven to be effective for HCHO oxidation at low temperatures, a high loading of Pt is generally required, which greatly limits its widespread application due to the expensive cost of platinum. Therefore, the reduction of Pt loading in Pt/TiO<sub>2</sub> catalysts is of great significance. Nie *et al.*<sup>56</sup> found that HCHO can be decomposed efficiently at room temperature over Pt/honeycomb ceramics (HC) with ultra-low Pt content. The activity of the Pt/HC catalysts is increased with increasing Pt loading in the range of 0.005–0.013 wt.% while further increasing Pt loading does not obviously improve its catalytic activity. Huang and Leung<sup>35</sup> reported that a series of supported Pt catalysts with low Pt loading developed by sodium borohydride (NaBH<sub>4</sub>) reduction are highly active in the elimination of indoor HCHO at ambient temperature. HCHO conversion reached nearly 100% on the reduced Pt/TiO<sub>2</sub> catalysts even with 0.1% Pt loading while it was less than 25% on PtO<sub>x</sub>/TiO<sub>2</sub>. Their assumption suggests that the negatively charged metallic Pt nanoparticles can facilitate the electron transfer and the formation of active oxygen which provides the active sites for HCHO oxidation. The same authors confirmed the supposition by studying the effects of different reduction treatments on structural properties and catalytic activity.<sup>57</sup> XPS results show that the binding energies (BEs) of 1% Pt/TiO<sub>2</sub>-IMP-NaBH<sub>4</sub> and 1% Pt/TiO<sub>2</sub>-IMP-H<sub>2</sub> catalysts were 70.2 eV and 70.8 eV, respectively, which were far away from the BEs of Pt<sup>2+</sup> and Pt<sup>4+</sup> but close to that of Pt<sup>0</sup>, indicating that Pt nanoparticles are reduced to the metallic state. The reduced Pt/TiO<sub>2</sub> catalysts with metallic Pt obtained much higher HCHO conversion than the unreduced ones with cationic Pt in all cases, again suggesting that the Pt oxidation state should be crucial to the catalytic activity. Although Huang and Leung<sup>35</sup> observed the phenomena that NaBH<sub>4</sub> reduction treatment greatly promoted the catalytic activity of Pt/TiO<sub>2</sub>, they failed to notice the favorable effect of residual sodium of the catalyst on HCHO oxidation. Recently, Zhang *et al.*<sup>58</sup> reported a novel alkali-metal-promoted Pt/TiO<sub>2</sub> catalyst for HCHO oxidation at ambient temperature and discussed the effect of alkali-metal ions (such as Li<sup>+</sup>, Na<sup>+</sup>, and K<sup>+</sup>) on the performance of Pt/TiO<sub>2</sub> catalysts. Surface hydroxyl species were supposed to be produced by water vapor in the system and the addition of alkali-metal ions improved the OH activation by stabilizing an atomically dispersed Pt–O(OH)<sub>x</sub>–alkali-metal species on the catalyst surface. A new reaction pathway for the HCHO oxidation at low temperature was provided, that is, the direct oxidation of formate, and the reaction between surface hydroxyls and formate is preferred over the decomposition of formate to CO followed by CO oxidation. Nie *et al.*<sup>59</sup> also confirmed that the

promotion effect of alkali ions over Pt/TiO<sub>2</sub> prepared through combined NaOH-assisted impregnation and NaBH<sub>4</sub>-reduction methods. Pt/TiO<sub>2</sub> catalysts prepared with the assistance of NaOH showed higher HCHO oxidation activity than those without NaOH due to the introduction of additional surface hydroxyl groups and the enhanced capacity toward HCHO adsorption.

Besides TiO<sub>2</sub>, other kinds of supports such as Fe<sub>2</sub>O<sub>3</sub> and MnO<sub>2</sub> were also used to support Pt for HCHO oxidation. Pt/Fe<sub>2</sub>O<sub>3</sub>, prepared by a colloid deposition route, was investigated for complete HCHO oxidation.<sup>60,61</sup> It was found that the catalysts exhibited better catalytic activity and stability at a lower calcination temperature. The crucial formation of Pt–O–Fe bonds shows a suitable interaction between Pt nanoparticles and iron oxide support. Yu and Wang<sup>62</sup> reported nanostructured Pt/MnO<sub>2</sub> catalysts with cocoon-, urchin-, and nest-like morphologies synthesized by a facile method. Among them, 2 wt.% Pt/nest-like MnO<sub>2</sub> showed the best catalytic performance and can reach 100% HCHO conversion at 70 °C. On the contrary, it was supposed to be heated up to 200 °C for a complete HCHO oxidation over Pt-free MnO<sub>2</sub> materials. The highly dispersed Pt nanoparticles and their synergistic effect with nanostructured MnO<sub>2</sub> support are responsible for the observed high catalytic activity over Pt/nest-like MnO<sub>2</sub>. Mixed oxides like MnO<sub>x</sub>–CeO<sub>2</sub> were used to support Pt catalysts for catalytic oxidation of HCHO.<sup>63</sup> Results show that the Pt precursors and reduction temperature significantly affected the catalytic performance of the Pt/MnO<sub>x</sub>–CeO<sub>2</sub> catalysts. The catalyst prepared from a chlorine-free precursor and reduction at 473 K with hydrogen showed extremely high catalytic activity and could completely oxidize HCHO to CO<sub>2</sub> and H<sub>2</sub>O at ambient temperature, while no deactivation was observed even after the reaction took 120 h.

### 3.2. Pd-based catalysts

Furthermore, palladium is also extensively used as an active component in several industrial catalytic formulations for the removal of air pollutants. As compared with platinum, palladium is generally more active in methane oxidation but worse in the transformation of other chemicals.<sup>64–68</sup> In addition, the palladium catalyst exhibited good resistance to thermal and hydrothermal sintering<sup>69</sup> and their price is relatively low. Thus, considerable attention has been given to the development of Pd catalysts for catalytic oxidation of VOCs in the past.<sup>70,71</sup>

Huang *et al.*<sup>70</sup> prepared a series of  $\gamma$ -Al<sub>2</sub>O<sub>3</sub> supported noble metals (Pd, Pt, Au, Ag, Rh) by wet impregnation and applied them in the catalytic oxidation of *o*-xylene. Among them, Pd/Al<sub>2</sub>O<sub>3</sub> is the most active. The nature of supports of Pd catalysts is crucial to the catalytic activity of VOC oxidation, which is similar to the behavior of supported Pt catalysts. Álvarez-Gálvan *et al.*<sup>72</sup> prepared Al<sub>2</sub>O<sub>3</sub> supported manganese and palladium–manganese oxide catalysts for the combustion of HCHO. The light-off temperature for the

Mn/Al<sub>2</sub>O<sub>3</sub> catalyst is 220 °C while it was drastically decreased to 90 °C over bimetallic 0.1% Pd–Mn/Al<sub>2</sub>O<sub>3</sub> and 80 °C over 0.4% Pd–Mn/Al<sub>2</sub>O<sub>3</sub> catalysts. The better performance of the Pd catalysts is attributed to the fact that PdO provides not only oxygen but also some metallic sites for the VOC decomposition. Okumura *et al.*<sup>73</sup> studied the effect of acid–base properties of metal oxide supported Pd catalysts. The proceeding discovery showed that 0.5 wt.% Pd/ZrO<sub>2</sub> exhibited the best performance during the catalytic oxidation of toluene. The Pd with strong acidic or basic support obtained lower catalytic activity than that with weak ones. Therefore, it was considered that the oxidation activity of Pd was controlled by the acid–base properties of the support through the electronic interaction between support and Pd. Especially, the tendency was remarkably pronounced on ZrO<sub>2</sub> calcined at high temperature due to the reduction in the acidic content of the ZrO<sub>2</sub> surface. Therefore, the facile generation of metallic Pd on these supports was responsible for the high activity in the total oxidation of toluene.

Li *et al.*<sup>74</sup> prepared a series of novel Pd/Co<sub>3</sub>AlO catalysts derived from hydrotalcite-like compounds (HTlcs) and used for total oxidation of toluene. The HTlc phase Co–Al precursors were prepared by coprecipitation and Pd active species were introduced by different approaches, *i.e.*, impregnation (IMP), wet ion exchange (WIE) or directly at the coprecipitation stage (COP). The discovery showed that all hydrotalcite-derived Pd/Co<sub>3</sub>AlO catalysts are much more active in toluene removal than the Pd/Co<sub>3</sub>AlO catalyst prepared *via* the traditional thermal combustion method (TCB). The activities of all synthesized catalysts obey the following sequence: Pd/Co<sub>3</sub>AlO (COP) > Pd/Co<sub>3</sub>AlO (WIE) ≥ Pd/Co<sub>3</sub>AlO (IMP) > Pd/Co<sub>3</sub>AlO (TCB). The excellent catalytic activities of the novel hydrotalcite-derived Pd/Co<sub>3</sub>AlO catalysts could be attributed to their high surface area, small mean crystallite size of support and highly dispersed PdO particles. Besides, they are well positively associated with the reduction ability of the catalyst and the amounts of oxygen vacancies.

Porous materials such as zeolites were also used to support Pd.<sup>75,76</sup> BEA and FAU zeolites were exchanged with

different cations in order to study the influence of alkali metal cations (Na<sup>+</sup>, Cs<sup>+</sup>) and H<sup>+</sup> in Pd-based catalysts with respect to the oxidation of propene and toluene. The exchange of the cations led to a decreased surface area and micropore volume. However, the reduction of pore size is beneficial to Pd dispersion, and this can promote the catalytic oxidation of VOCs. Total oxidation of toluene was achieved below 200 °C over the 0.5%Pd/NaFAU and 0.5%Pd/CsFAU catalysts. Novel Pd/hierarchical macro-mesoporous ZrO<sub>2</sub>, TiO<sub>2</sub> and ZrO<sub>2</sub>–TiO<sub>2</sub> with high surface areas have been synthesized and used as supports of Pd for toluene oxidation.<sup>77</sup> Fig. 3 shows the TEM images of the macro-mesoporous mixed oxide. The prepared Pd catalysts were highly active and the *T*<sub>90%</sub> of catalytic oxidation of toluene was obtained at a temperature as low as 150 °C. Pd<sup>0</sup> was initially oxidized by O<sub>2</sub> to form very active [Pd<sup>2+</sup>O<sup>2−</sup>] species and the Pd<sup>2+</sup> cation was simultaneously reduced to Pd<sup>0</sup> as toluene was oxidized by active [Pd<sup>2+</sup>O<sup>2−</sup>] species.

The valence state of Pd of supported Pd catalysts remained controversial during the combustion of all the VOCs.<sup>78,79</sup> Some authors proposed that metallic species (Pd<sup>0</sup>) are active sites for catalytic oxidation<sup>70,79,80</sup> while the others affirmed that the oxide formed (PdO/Pd<sup>2+</sup>) should be the active one.<sup>81,82</sup> It is generally difficult to distinguish the state of Pd since Pd can readily undergo oxidation/reduction transformations (Pd ↔ PdO) during VOC catalytic combustion at high temperature and these transformations might affect the catalytic activity for VOC oxidation.<sup>79,83</sup> This led to the confusion of the effect of the Pd valence state.<sup>84</sup> The transformations of Pd/PdO would not happen since the Pd state can be kept unchanged at temperatures that are lower than 180 °C.<sup>70,79</sup> It can be easier and clearer to distinguish the catalytic activity of metallic Pd and PdO during catalytic oxidation of HCHO at room temperature. Huang and Leung<sup>84</sup> prepared a series of reduced and oxidized Pd/TiO<sub>2</sub> catalysts. The reduced catalysts were much more active than the oxidized ones. Nearly 100% HCHO conversion was achieved by the former catalyst while the latter one got less than 18%. HCHO catalytic oxidation was successfully obtained at room temperature for the

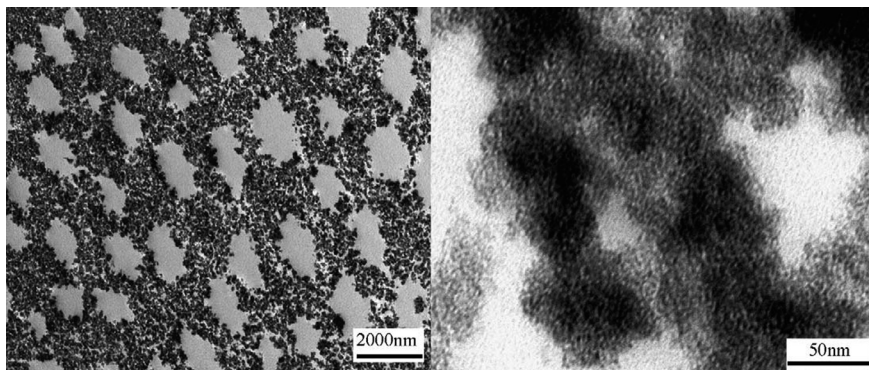


Fig. 3 TEM images of macro-mesoporous mixed oxide.<sup>77</sup> (Reprinted with permission from H. L. Tidahy, S. Siffert, J. F. Lamonier, E. A. Zhilinskaya, A. Aboukais, Z. Y. Yuan, A. Vantomme, B. L. Su, X. Canet, G. De Weireld, M. Frère, T. B. N'Guyen, J. M. Giraudon and G. Leclercq, *New Pd/hierarchical macro-mesoporous ZrO<sub>2</sub>, TiO<sub>2</sub> and ZrO<sub>2</sub>–TiO<sub>2</sub> catalysts for VOCs total oxidation*, *Appl. Catal., A*, 2006, **310**, 61–69. Copyright 2006, Elsevier).



first time over the  $\text{NaBH}_4$  reduced  $\text{Pd/TiO}_2$ . Well-dispersed and negatively charged metallic Pd nanoparticles were generated, and should be the active sites due to the strong capacity for oxygen activation. The capability of the  $\text{Pd/TiO}_2$  catalysts to activate the chemisorbed oxygen is also a critical factor that determines their catalytic activity apart from their capacity to generate chemisorbed oxygen. In another work, the author revealed water vapor promoted HCHO oxidation over  $\text{Pd/TiO}_2$  catalysts,<sup>85</sup> which is different from the detrimental effect of water vapor on catalytic oxidation of BTX over  $\text{Pt/Al}_2\text{O}_3$ .<sup>49</sup> Actually, water vapor is essential to HCHO oxidation since the hydroxyl radical from water vapor dissociation favors the adsorption and transfer of oxygen on the  $\text{Pd/TiO}_2$  catalysts.

Chlorine is generally considered as a poison to noble metal catalysts for catalytic oxidation of VOCs since it will block metallic active sites. Moreover, the active noble metal will be transferred into less active oxychlorinated species,  $\text{MO}_x\text{Cl}_y$ , in the presence of chlorine.<sup>15</sup> The inhibition phenomenon was also observed in room temperature catalytic oxidation of HCHO over  $\text{H}_2$  reduced  $\text{Pd/TiO}_2$  catalysts. However, the  $\text{NaBH}_4$  reduced  $\text{Pd/TiO}_2$  was kept highly active during the catalytic oxidation of HCHO at room temperature in the presence of chlorine.<sup>84</sup> The discrepancy in susceptibility to chlorine inhibition on different catalysts and in different reactions is probably caused by unlike preparation methods and reaction conditions.

Based on the alkali ion promotion effect on the catalytic activity of noble metal based catalysts, Zhang *et al.*<sup>86</sup> reported the issue of using sodium-doped  $\text{Pd/TiO}_2$  catalysts for HCHO oxidation. It was observed that Na doping has dramatically promoted the catalytic activity of  $\text{Pd/TiO}_2$  catalysts. Nearly 100% HCHO conversion could be achieved over the  $2\text{Na-Pd/TiO}_2$  catalyst at 25 °C. The results showed that the addition of Na species can induce the formation and stabilization of a negatively charged and well-dispersed Pd species which facilitates the activation of surface OH groups and chemisorbed oxygen. This is responsible for the high performance of the  $2\text{Na-Pd/TiO}_2$  catalyst in the ambient HCHO destruction.

### 3.3. Au-based catalysts

As a symbol of wealth and power, gold has strongly attracted the attention of human beings for thousands of years. In the field of catalysis, gold has long been considered as inactive because of its chemical inertness. However, since Haruta *et al.*<sup>87</sup> discovered that when gold nanoparticles are dispersed on metal oxides they become exceptionally active for low temperature CO oxidation. Gold nanoparticles, as new catalytic materials, had exhibited unpredictable and unique catalytic properties to the world, and have aroused people's great interest.

To the best of our knowledge, the first significant papers that deal with VOC combustion over gold catalysts appeared later in 1995 and 1996.<sup>88–90</sup> This suggests the high activity of  $\text{Au/Co}_3\text{O}_4$  in the catalytic combustion of methane<sup>88</sup> and

chloromethane<sup>90</sup> and of  $\text{Au}/\alpha\text{-Fe}_2\text{O}_3$  in the catalytic oxidation of methanol, formaldehyde and formic acid.<sup>89</sup> Since then, gold nanoparticles which are supported by  $\text{Fe}_2\text{O}_3$ ,  $\text{Co}_3\text{O}_4$ ,  $\text{CeO}_2$ ,  $\text{TiO}_2$ , and  $\text{Mn}_2\text{O}_3$  have been extensively reported for VOC catalytic oxidation. Looking back to the pioneering work by Haruta, his early success should be attributed to the appropriate choice of preparation methods and carrier which led to a small and homogeneous gold nanoparticle size (<5 nm). The performance of gold catalysts for VOC oxidation is highly dependent on the size of gold particles as well as the nature of the support.<sup>91</sup> They are strongly affected by the preparation method and the pretreatment conditions.<sup>87,92–95</sup>

In a comparative study on iron oxide supported IB metals (Au, Ag, Cu) (Fig. 4), gold was the most active in VOC combustion and its catalytic activity greatly depended on the capacity to weaken the Fe–O bond. The weak Fe–O bond can increase the mobility of the lattice oxygen which is involved in the VOC oxidation probably through a Mars–van Krevelen mechanism.<sup>96</sup> Grisel *et al.*<sup>97</sup> compared the performance towards the methane total oxidation over  $\text{Au/Al}_2\text{O}_3$  catalysts that were prepared by impregnation (pore volume and wet) and deposition–precipitation with  $\text{Na}_2\text{CO}_3$  (DP) or urea (HDP) as precipitating agents. They found that the  $\text{Au/Al}_2\text{O}_3$  type prepared by deposition–precipitation showed a better catalytic activity than that prepared by impregnation. Specifically,  $\text{Au/Al}_2\text{O}_3$  prepared by HDP exhibited the highest catalytic activity since the smallest Au particles were obtained due to a slower and more homogeneous pH variation of the solution. The same authors<sup>98</sup> studied the effect of the support for  $\text{CH}_4$  over  $\text{Au/MO}_x/\text{Al}_2\text{O}_3$  ( $\text{M} = \text{Cr, Mn, Fe, Co, Ni, Cu, Zn}$ ) and found out that the catalytic activity highly depends on both the particle size and the type of  $\text{MO}_x$ . It followed the order:  $\text{CuO}_x > \text{MnO}_x > \text{CrO}_x > \text{FeO}_x > \text{CoO}_x > \text{NiO}_x > \text{ZnO}_x$ . It has also been claimed that the support is directly involved

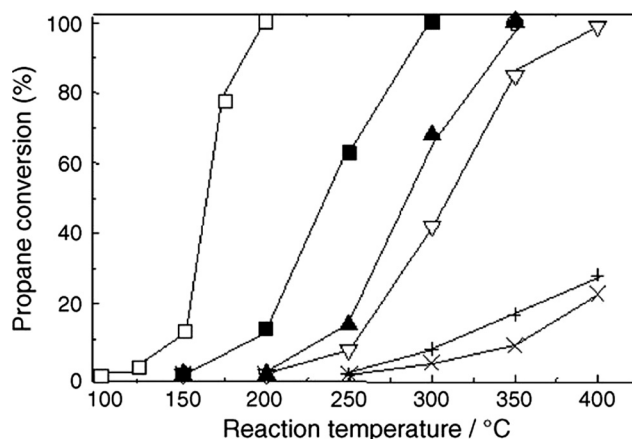


Fig. 4 Evolution of propane conversion with reaction temperature for propane combustion over metal oxide catalysts. Symbols: ( $\square$ )  $\text{CoO}_x$ , ( $\blacksquare$ )  $\text{MnO}_x$ , ( $\blacktriangle$ )  $\text{CuO}$ , ( $\nabla$ )  $\text{Fe}_2\text{O}_3$ , ( $\times$ )  $\text{CeO}_2$  and (+)  $\text{TiO}_2$ .<sup>101</sup> (Reprinted with permission from B. E. Solsona, T. Garcia, C. Jones, S. H. Taylor, A. F. Carley, G. J. Hutchings, Supported gold catalysts for the total oxidation of alkanes and carbon monoxide, *Appl. Catal., A*, 2006, **312**, 67–76. Copyright 2006, Elsevier).

in the reaction when reducible oxides are used as the support. Generally, the resulting anion vacancies and surface lattice oxygen that are close to the gold particles have been seen as the sites of oxygen adsorption and activation.<sup>7</sup> Scirè *et al.*<sup>96,99,100</sup> studied the total oxidation of methanol, 2-propanol, acetone and toluene over Au/iron oxide and pointed out the participation of the lattice oxygen of the support in the reaction. Solsona *et al.*<sup>101</sup> also compared the performance of Au catalysts which were supported on a series of metal oxides such as  $\text{CoO}_x$ ,  $\text{MnO}_x$ ,  $\text{CuO}_x$ ,  $\text{Fe}_2\text{O}_3$ ,  $\text{CeO}_2$  and  $\text{TiO}_2$ , for catalytic oxidation of methane, ethane and propane (Fig. 4). In the case of an Au/ $\text{CoO}_x$  catalyst, the total oxidation of propane was observed at a temperature that was as low as 200 °C. The presence of gold in the catalysts enhanced the reducibility of the support and a correlation between the redox properties of the catalysts and the catalytic activity has been established. In a more recent study, the same group confirmed the proposal over gold that is supported on high surface area cobalt oxide.<sup>102</sup>

$\text{CeO}_2$ , as the support of gold, has attracted increasing attention for catalytic oxidation of VOCs in recent years due to its strong oxygen storage capacity. Centeno *et al.*<sup>103</sup> investigated catalytic oxidation of *n*-hexane, benzene and 2-propanol by Au/ $\text{Al}_2\text{O}_3$  catalysts and found that the addition of  $\text{CeO}_2$  enhanced the fixation and final dispersion of gold particles, which led to the stabilization of gold particles with smaller crystallite size. In addition, the redox properties of  $\text{CeO}_2$  can increase the mobility of the lattice oxygen and provide an adequate oxidation state of gold. Similar phenomena were observed during the catalytic combustion of toluene over Au/ $\text{CeO}_2$  catalysts.<sup>104</sup> The catalysts that were prepared by the deposition-precipitation method showed better performance than those prepared by co-precipitation due to the formation of smaller gold particles. The presence of gold weakens the surface Ce–O bonds adjacent to the gold atoms, thus increasing the mobility and activity of surface lattice oxygen and affecting catalytic activity towards VOC oxidation. Ousmane *et al.*<sup>105</sup> compared catalytic oxidation towards total oxidation of propene and toluene over Au/ $\text{CeO}_2$ , Au/ $\text{TiO}_2$ , Au/ $\text{Al}_2\text{O}_3$  and Au/ $\text{CeO}_2\text{-Al}_2\text{O}_3$ . They found that Au/ $\text{CeO}_2$  was the most active (Fig. 5) and the nature of the support and its point of zero charge (PZC) affect the amount of deposited gold, which led to the highest conversion of propene and toluene on  $\text{CeO}_2$  with the lowest PZC values.

Various Au/ $\text{CeO}_2$  catalysts have also been extensively applied for HCHO oxidation due to their high activity.<sup>106</sup> Jia *et al.*<sup>107</sup> prepared a series of supported gold catalysts with different supports for catalytic oxidation of HCHO and CO. The catalyst derived from the as-precipitated hydroxide showed higher activity than that from the corresponding oxide support. Complete oxidation of HCHO occurred at 80 °C over Au/ $\text{CeO}_2$ . Another Au/ $\text{CeO}_2$  catalyst with gold below 0.85 wt.% was prepared by co-precipitation.<sup>108</sup> It can totally oxidize HCHO at temperatures close to 100 °C. The relation between the gold crystal structure and the performance of Au/ $\text{CeO}_2$  catalysts was proposed. The highly dispersed and poorly crystallized metallic

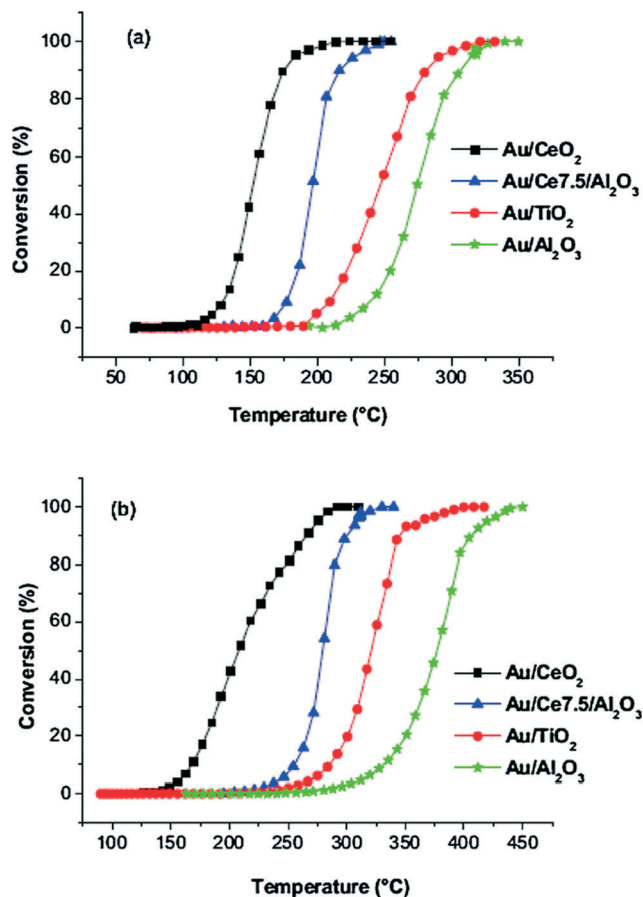


Fig. 5 Conversion (%) of (a) propene and (b) toluene versus temperature over gold supported catalysts (third catalytic run).<sup>105</sup> (Reprinted with permission from M. Ousmane, L. F. Liotta, G. Di Carlo, G. Pantaleo, A. M. Venezia, G. Deganello, L. Retailleau, A. Boreave and A. Giroir-Fendler, Supported Au catalysts for low-temperature abatement of propene and toluene, as model VOCs: Support effect, *Appl. Catal., B*, 2011, 101, 629–637. Copyright 2011, Elsevier).

gold and the small amount of oxidized gold exhibited superior catalytic activity towards HCHO oxidation when compared with large and well-crystallized particles that were calcined at higher temperatures. In addition, the high surface area of the Au/ $\text{CeO}_2$  catalysts is favorable to low-temperature oxidation of HCHO.<sup>109</sup> With the increased surface area of supports, Au nanoparticles mainly exist in high oxidation states which can provide strong capacity for HCHO adsorption and promote HCHO catalytic oxidation. HCHO conversion of 92.3% was obtained at 37 °C over the 3.0 wt.% Au/ $\text{CeO}_2$  catalyst with a surface area of 270 m<sup>2</sup> g<sup>-1</sup>.

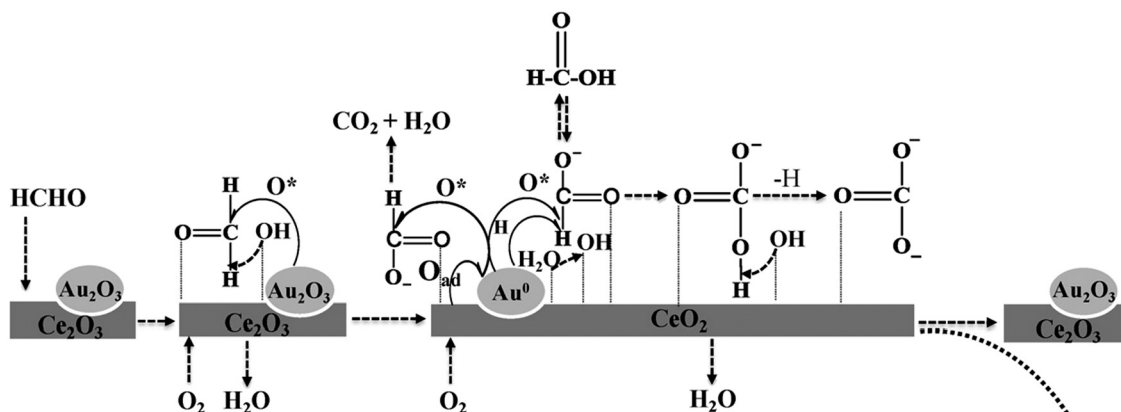
Besides Au/ $\text{CeO}_2$ , Au/ $\text{FeO}_x$  was also prepared for catalytic oxidation of HCHO.<sup>110,111</sup> Li *et al.*<sup>110</sup> found that the Au/ $\text{FeO}_x$  catalyst containing 7.10 wt.% gold exhibited the highest catalytic activity. On this catalyst, catalytic oxidation of HCHO occurred at 20 °C and complete burn-off of HCHO was achieved at 80 °C. The catalysts were stable and remained active in the presence of moisture. XPS characterization revealed that Au5d electrons partially flew into the Fe 3d orbital or into its 6s orbital. The strong interaction between

metal and support also greatly affected the catalytic activity of gold nanoparticles. Zhu *et al.*<sup>112</sup> prepared gold catalysts loaded on the porous nanocomposite of  $\text{ZrO}_2$  and  $\text{SiO}_2$  by deposition-precipitation and used them for HCHO catalytic oxidation. It was found that gold was reduced from an oxidized state of  $\text{Au}^{3+}$  to metallic crystals ( $\text{Au}^0$ ) during the reaction. The gold species in both states are the active sites for HCHO oxidation since HCHO oxidation involves a reaction between adsorbed formate species and oxygen molecules. HCHO adsorption on the gold species and oxygen adsorption on the support are crucial steps for the oxidation.

Recently, Zhang *et al.*<sup>113,114</sup> successfully developed a new synthetic route to obtain three-dimensionally ordered macroporous (3DOM)  $\text{Au}/\text{CeO}_2$  and (3DOM)  $\text{Au}/\text{CeO}_2\text{-Co}_3\text{O}_4$  catalysts. The three-dimensionally ordered macroporous support  $\text{CeO}_2$  and  $\text{CeO}_2\text{-Co}_3\text{O}_4$  materials with controlled pore sizes were firstly prepared *via* a colloidal crystal template method and then gold nanoparticles were incorporated into the support by the gas bubbling-assisted deposition precipitation method. The as-prepared (3DOM)  $\text{Au}/\text{CeO}_2$  and (3DOM)  $\text{Au}/\text{CeO}_2\text{-Co}_3\text{O}_4$  catalysts can achieve total HCHO oxidation

at 75 °C and 39 °C, respectively, which are much lower than other reported  $\text{Au}/\text{CeO}_2$  catalysts.<sup>108</sup> The good dispersion of Au nanoparticles and mixed valence states of  $\text{Au}^{3+}$  and  $\text{Au}^0$  can be responsible for the high catalytic activity on (3DOM)  $\text{Au}/\text{CeO}_2$  and (3DOM)  $\text{Au}/\text{CeO}_2\text{-Co}_3\text{O}_4$ . Compared with (3DOM)  $\text{Au}/\text{CeO}_2$ , (3DOM)  $\text{Au}/\text{CeO}_2\text{-Co}_3\text{O}_4$  exhibited better catalytic activity, indicating that the synergistic effect between  $\text{CeO}_2$  and  $\text{Co}_3\text{O}_4$  supports can significantly accelerate the surface active oxygen migration and activate Au species. Subsequently, two catalytic mechanisms of enhanced HCHO catalytic oxidation over the 3DOM  $\text{Au}/\text{CeO}_2$  catalyst were proposed based on  $\text{H}_2$ -TPR, HCHO TPSR,  $\text{CO}_2$ -TPD, and FT-IR characterization, as shown in Fig. 6.<sup>115</sup> The weak absorption ability of  $\text{CO}_2$  over 3DOM  $\text{Au}/\text{CeO}_2$  and the existence of Au active species in ionic and metallic states in the 3DOM  $\text{Au}/\text{CeO}_2$  catalyst greatly improved the catalytic activity. Interestingly, the process on  $\text{Au}^{3+}$  showed higher activity than that on  $\text{Au}^0$ , which is different from the trend observed in other noble metals like Pt and Pd mentioned above. Metallic Pt and Pd were supposed to be more active than cationic ones while it involves the participation of both  $\text{Au}^{3+}$  and  $\text{Au}^0$  in the

### Mechanism 1: HCHO catalytic oxidation by $\text{Au}^{3+}$



### Mechanism 2: HCHO catalytic oxidation by $\text{Au}^0$

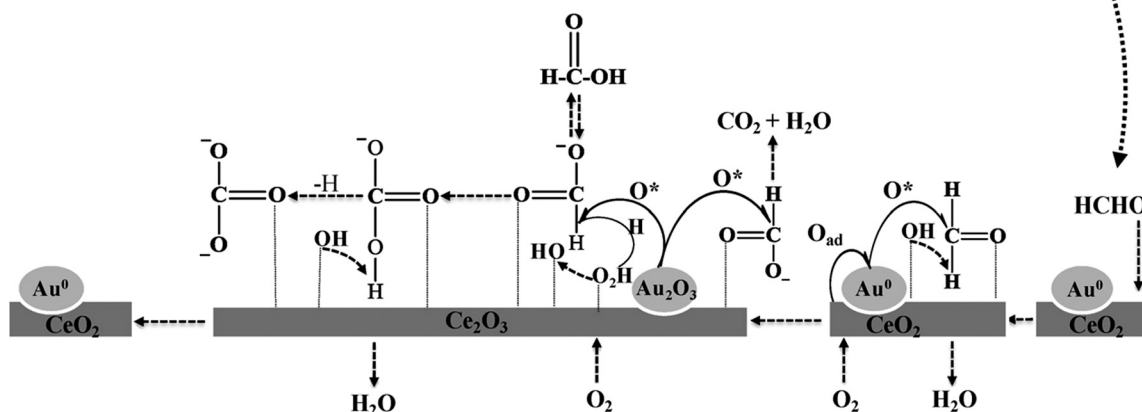


Fig. 6 The proposed catalytic mechanism of 3DOM  $\text{Au}/\text{CeO}_2$  catalyst for enhanced HCHO catalytic oxidation.<sup>115</sup> (Reprinted with permission from B. Liu, C. Li, Y. Zhang, Y. Liu, W. Hu, Q. Wang, L. Han and J. Zhang, Investigation of catalytic mechanism of formaldehyde oxidation over three-dimensionally ordered macroporous  $\text{Au}/\text{CeO}_2$  catalyst, *Appl. Catal., B*, 2012, 111–112, 467–475. Copyright 2012, Elsevier).

HCHO oxidation. So, it remains a matter of debate between oxidation states of noble metals and their catalytic performance.<sup>116</sup>

Three-dimensionally ordered mesoporous  $\text{Co}_3\text{O}_4$  was also prepared to support gold catalysts.<sup>117</sup> The higher surface area and oxygen adspecies concentration, better low-temperature reducibility, and the strong interaction between Au and meso- $\text{Co}_3\text{O}_4$  were responsible for the excellent catalytic performance of 6.5% Au/meso- $\text{Co}_3\text{O}_4$ , which can achieve the  $T_{90\%}$  (the temperature required for achieving a conversion of 90%) for the oxidation of CO, benzene, toluene, and *o*-xylene at temperatures as low as  $-45^\circ\text{C}$ ,  $189^\circ\text{C}$ ,  $138^\circ\text{C}$ , and  $162^\circ\text{C}$ , respectively (Fig. 7).

Gold bimetallic nanocatalysts represent another attractive research field for VOC catalytic oxidation in the past decade.<sup>44,118,119</sup> These types of catalysts have shown better capabilities in structure and chemical composition than the single-metal analogues, and thus provide more possibilities for the improved activity, selectivity and stability.<sup>120</sup> Bimetallic Pt–Au catalysts supported on  $\text{ZnO}/\text{Al}_2\text{O}_3$  were prepared for toluene oxidation and the lowest  $T_{80\%}$  is obtained at  $182^\circ\text{C}$

while it was increased to  $195^\circ\text{C}$  for Pt monometallic catalysts. TPR results showed that nanosized gold particles greatly promoted the reduction of surface oxygen at lower temperatures.<sup>44</sup>

It is worth noting that gold and platinum on the nano-scale show different behavior during the catalytic oxidation of VOCs, although both metals bind reactants more strongly as the particle size becomes smaller.<sup>44</sup> The binding of reactants with Pt becomes so strong that the reaction never proceeds at low temperatures. As for gold, however, the weaker binding and flexibility of the nanoparticles promotes catalytic reaction. Finally, it was experimentally discovered that Au particles which are smaller than 5 nm are more active than other noble-metal catalysts for reactions. In contrast, Pt particles that are smaller than 5 nm are less catalytically active.<sup>44</sup>

### 3.4. Ag-based catalysts

In early 1993, Imamura *et al.*<sup>121</sup> found that both silver–cerium composite oxide and  $\text{CeO}_2$  were active for HCHO oxidation. IR analysis revealed that intermediate species like

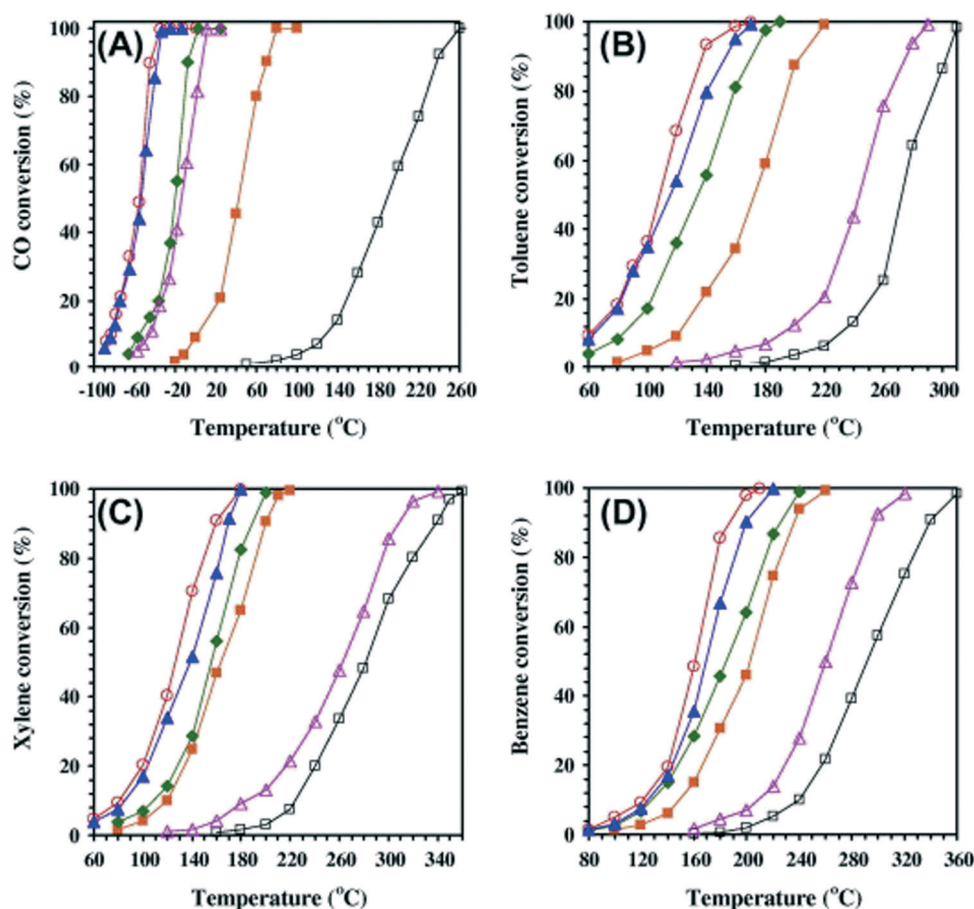


Fig. 7 (A) CO, (B) toluene, (C) *o*-xylene, and (D) benzene conversions as a function of temperature over (■) meso- $\text{Co}_3\text{O}_4$ , (◆) 3.7 Au/meso- $\text{Co}_3\text{O}_4$ , (○) 6.5 Au/meso- $\text{Co}_3\text{O}_4$ , (▲) 9.0 Au/meso- $\text{Co}_3\text{O}_4$ , (□) bulk  $\text{Co}_3\text{O}_4$ , and (△) 6.4 Au/bulk  $\text{Co}_3\text{O}_4$  under the conditions of CO concentration = 1.0 vol.%, CO/ $\text{O}_2$  molar ratio = 1/20, and SV = 60 000  $\text{mL} (\text{g}^{-1} \text{h}^{-1})$  or VOC (benzene, toluene or *o*-xylene) concentration = 1000 ppm, VOC/ $\text{O}_2$  molar ratio = 1/400, and SV = 20 000  $\text{mL} (\text{g}^{-1} \text{h}^{-1})$ .<sup>117</sup> (Reprinted with permission from Y. Liu, H. Dai, J. Deng, S. Xie, H. Yang, W. Tan, W. Han, Y. Jiang and G. Guo, Mesoporous  $\text{Co}_3\text{O}_4$ -supported gold nanocatalysts: highly active for the oxidation of carbon monoxide, benzene, toluene, and *o*-xylene, *J. Catal.*, 2014, **309**, 408–418. Copyright 2014, Elsevier).



methoxide, dioxymethylene, and/or polyoxymethylene were produced even at room temperature. However, bi-carbonate and formate were formed only on silver–cerium composites and  $\text{CeO}_2$ , respectively. These intermediates suffered further oxidation at higher temperatures (100 °C and 150 °C) easily on Ag– $\text{CeO}_2$  composite catalysts but are rather difficult on  $\text{CeO}_2$ . Mao *et al.*<sup>122</sup> studied HCHO oxidation on silver catalysts supported on  $\alpha\text{-Al}_2\text{O}_3$  and  $\text{SiO}_2$  with high surface area. All the supported Ag catalysts were active above 200 °C while significant deactivation occurred at lower temperatures. Chen *et al.*<sup>123</sup> studied the adsorption and surface reaction activity of HCHO on the Ag/MCM-41 catalysts with different silver loadings by temperature programmed desorption (TPD) and temperature programmed surface reaction (TPSR) methods. It appeared that silver loading imposed great influence on the adsorption and surface reaction activity of HCHO. The addition of silver provided a new adsorption site for the HCHO molecules at low temperature, and its desorption temperature moved to lower temperature with increased silver loading to 8 wt.% while the desorption temperature of HCHO shifted to higher temperatures with further increase in silver loading. This suggests that an appropriate silver loading and particle dispersion are essential to high catalytic activity for HCHO oxidation. Compared with impregnated Ag/SBA-15, monodispersed Ag nanoparticles prepared by the post-grafting method exhibited higher dispersion, smaller particle size and narrower size distribution, thus leading to better catalytic activity for HCHO oxidation. HCHO can be completely oxidized to harmless products over monodispersed Ag at about 100 °C.<sup>124</sup>

$\text{MnO}_x\text{-CeO}_2$  was also used to support silver for catalytic oxidation of HCHO.<sup>125</sup> The addition of silver species greatly improved the activation of oxygen molecules and complete oxidation of HCHO was obtained at a temperature as low as 100 °C. A mechanism was proposed that the consecutive oxygen transfer starts from the oxygen reservoir of  $\text{CeO}_2$  to the active  $\text{Ag}_2\text{O}$  sites through  $\text{MnO}_x$ .

Three-dimensional (3D) ordered mesoporous Ag/ $\text{Co}_3\text{O}_4$  was successfully prepared on the basis of 3D- $\text{Co}_3\text{O}_4$  and it was found that the addition of  $\text{K}^+$  ions could promote catalytic activity.<sup>126</sup> The increased catalytic activity toward HCHO oxidation is ascribed to surface  $\text{OH}^-$  species provided by  $\text{K}^+$  ions and more abundant Ag(111) active facets,  $\text{Co}^{3+}$  cations and surface lattice oxygen ( $\text{O}^{2-}$ ) species generated by stronger interaction between Ag, Co and anion lattice defects.

It is clear that the quantity or volume of the interfacial oxygen and the particle size of Ag play a crucial role in regulating catalytic activity. Hence, it is highly desirable to down-size silver nanoparticles to clusters or even to single atoms in order to enhance catalytic activities. Tang *et al.*<sup>127</sup> successfully prepared single-atom Ag chains on the support of hollandite-type manganese oxide nanorods. This single-atom Ag catalyst exhibited excellent activation ability to both lattice oxygen and molecular dioxygen at low temperatures. It can completely oxidize HCHO below 80 °C. The formation of a

single-atom Ag chain and the detailed mechanism of VOC oxidation over it remain an interesting field to be explored.

## 4. Transition metal oxide catalyst

Compared with the expensive and scarce noble metals, transition metal oxide catalysts are much cheaper. They are feasible and sufficiently active in some reactions. Great efforts have been made in order to develop efficient transition metal oxide catalysts for VOC catalytic oxidation for the purpose of replacing noble metal catalysts and the reduction of the reaction temperature.

P-type metal oxides are generally active oxidation catalysts since they are electron-deficient in the lattice and conduct electrons by means of positive “holes”.<sup>25</sup> The difference between these mechanisms for the two types of oxides, p-type oxides involving adsorbed  $\text{O}^-$  and n-type oxides involving lattice  $\text{O}^{2-}$ , leads to profoundly different activity for deep oxidation reactions. The p-type oxides are generally more active, especially for deep oxidation, since the adsorbed oxygen species are more reactive than the lattice oxide ions.<sup>25</sup> Therefore, the developed transition metal oxide catalysts are mainly focused on p-type oxides. A recent study showed that catalytic materials with the same composition but different structures or morphology show diverse catalytic activity for the preferential exposure of different active sites.<sup>128–130</sup>

A summary of the main literature data on the catalytic oxidation of VOCs over transition metal oxides at low temperature discussed in this review is provided in Table 2.

### 4.1. Manganese oxides

Among the various different transition-metal oxides,  $\text{MnO}_x$  should be the most extensively studied because of its high activity, durability, and low toxicity as well as some unique chemical and physical properties. In 2001, Sekine *et al.*<sup>131</sup> developed a board-like air-cleaning material consisting of activated carbon particles and manganese oxides, by which HCHO could be decomposed into carbon dioxide even at room temperature. They continued their studies on HCHO removal over several metal oxides in a static reaction vessel.<sup>132</sup> Among these metal oxides,  $\text{Ag}_2\text{O}$ , PdO, CoO,  $\text{MnO}_2$ ,  $\text{TiO}_2$ ,  $\text{CeO}_2$  and  $\text{Mn}_3\text{O}_4$  showed relatively high HCHO removal efficiencies (over 50%) and  $\text{MnO}_2$  obtained the highest efficiency of 91%.

In general, manganese oxides have a considerably wide range of crystal phases ( $\beta\text{-MnO}_2$ ,  $\gamma\text{-MnO}_2$ ,  $\alpha\text{-Mn}_2\text{O}_3$ ,  $\gamma\text{-Mn}_2\text{O}_3$ ,  $\alpha\text{-Mn}_3\text{O}_4$ , and  $\text{Mn}_5\text{O}_8$ ) and are present in the form of 1-D tunnel structures, 2-D layer phases, and 3-D spinels. Moreover, manganese atoms have various oxidation states (+2, +3, +4). The strong ability to switch oxidation states and form structural defects is beneficial to high oxygen mobility and oxygen storage.<sup>133</sup>

Catalytic oxidation of benzene and toluene was studied over a series of manganese oxide catalysts ( $\text{Mn}_3\text{O}_4$ ,  $\text{Mn}_2\text{O}_3$  and  $\text{MnO}_2$ ) and the  $\text{Mn}_3\text{O}_4$  catalysts promoted with K, Ca and Mg.<sup>134</sup> The sequence of catalytic activity was found as

**Table 2** Survey of literature data on catalytic oxidation of VOCs over transition metal oxides at low temperature<sup>a</sup>

Catalyst	Preparation method	VOC type	Reaction mixture	$T_{90\%}$ , °C	Ref.
Rod-like $\alpha$ -MnO <sub>2</sub> Tube-like $\alpha$ -MnO <sub>2</sub> Flower-like Mn <sub>2</sub> O <sub>3</sub> Wire-like $\alpha$ -MnO <sub>2</sub>	Hydrothermal method	HCHO	1000 ppm toluene Toluene/O <sub>2</sub> = 1/4 N <sub>2</sub> balance	<250	129
Mn <sub>3</sub> O <sub>4</sub> Mn <sub>2</sub> O <sub>3</sub> MnO <sub>2</sub> MnO <sub>x</sub>	Calcination	Benzene Toluene	1000 ppm Air balance	<250	134
	Reflux method	Ethanol Ethyl acetate Toluene	4000 mg C m <sup>-3</sup>	208 206 258	135
$\gamma$ -MnO <sub>2</sub>	Purchased	Trimethylamine <i>n</i> -Hexane	250 ppm trimethylamine 125 ppm <i>n</i> -hexane	<200	136
Pyrolusite Cryptomelane Todorokite OMS-2	Redox hydrothermal method	HCHO	400 ppm HCHO 10% O <sub>2</sub> , N <sub>2</sub> balance	<180 <140 <160	137
	Reflux method	Ethanol Acetaldehyde	300 ppm ethanol 100 ppm acetaldehyde 10% O <sub>2</sub> , N <sub>2</sub> balance	<140 <100	138
OMS-2	Reflux method	HCHO	%HCHO 20% O <sub>2</sub> , He balance	<80	139
K-OMS-2	Soft chemistry route	HCHO	460 ppm HCHO Air balance	RT	140
Hollow MnO <sub>2</sub> Honeycomb MnO <sub>2</sub>	Soft chemistry route	HCHO	100 ppm HCHO 20% O <sub>2</sub> , He balance	<80 <90	141
Mn <sub>3</sub> O <sub>4</sub> Nano-Co <sub>3</sub> O <sub>4</sub> 2D-Co <sub>3</sub> O <sub>4</sub> 3D-Co <sub>3</sub> O <sub>4</sub> Ordered mesoporous Co <sub>3</sub> O <sub>4</sub>	Hydrothermal method Nanocasting	Benzene HCHO	Air balance 400 ppm HCHO 20% O <sub>2</sub> , N <sub>2</sub> balance	<300 <220 <140 <120	142 144
	Nanocasting	Ethylene	50 ppm ethylene 22% O <sub>2</sub> , N <sub>2</sub> balance	—	145
CeO <sub>2</sub>	Thermal decomposition	TCE	1000 ppm Air balance	<250	148
MnO <sub>x</sub> -CeO <sub>2</sub>	Urea-nitrate combustion	Ethanol Toluene Ethyl acetate Acetic acid	1600 ppm ethanol 600 ppm toluene 1800 ppm ethyl acetate 1400 ppm acetic acid 20% O <sub>2</sub> /He	<250 <250 <250 <200	149
MnO <sub>x</sub> -CeO <sub>2</sub>	Sol-gel CP Modified CP CP	HCHO	580 ppm HCHO 18% O <sub>2</sub> , He balance	<180 <160 <100	151
CeO <sub>2</sub> CeMn10 CeMn30 CeMn50 CeMn80 MnO <sub>x</sub> MnO <sub>x</sub> /ZrO <sub>2</sub> MnO <sub>x</sub> /Fe <sub>2</sub> O <sub>3</sub> MnO <sub>x</sub> /CoO <sub>x</sub> MnO <sub>x</sub> /CuO <sub>x</sub>		HCHO	580 ppm HCHO 20% O <sub>2</sub> , N <sub>2</sub> balance	<250 <150 <150 <100 <100 <100 <250	152
	Reverse microemulsion	Toluene	0.35% toluene 9% O <sub>2</sub> , Ar balance	<250	153

<sup>a</sup> IMP: impregnation, DP: deposition-precipitation, CP: co-precipitation, RT: room temperature.

follows: Mn<sub>3</sub>O<sub>4</sub> > Mn<sub>2</sub>O<sub>3</sub> > MnO<sub>2</sub>, which was closely correlated with the oxygen mobility on the catalyst. The addition of potassium (K), calcium (Ca) or magnesium (Mg) to Mn<sub>3</sub>O<sub>4</sub> enhanced the catalytic activity while the promoting effect might be ascribed to the defect-oxide or hydroxyl-like groups.

Santos *et al.*<sup>135</sup> studied the role of lattice oxygen in catalytic activity of manganese oxides towards the oxidation of ethanol, ethyl acetate and toluene. Among the manganese oxides tested, cryptomelane (KMn<sub>8</sub>O<sub>16</sub>) was found to be very active in VOC oxidation. The performance of cryptomelane

was significantly affected by the presence of other phases, namely, Mn<sub>2</sub>O<sub>3</sub> and Mn<sub>3</sub>O<sub>4</sub>. Mn<sub>3</sub>O<sub>4</sub> improves catalytic performance due to the increased reactivity and mobility of lattice oxygen while Mn<sub>2</sub>O<sub>3</sub> imposes the opposite effect. It is clear that there is a correlation between the redox properties and catalytic activity of the manganese oxides. In addition, catalytic oxidation of VOCs was influenced by the type of organic compound as each VOC affects the reduction of the catalyst and, consequently, the incorporation rate of oxygen from the gas phase. The removal efficiency of VOCs under the same

conditions followed the order: toluene < ethanol < ethyl acetate. Toluene has the lowest conversion since it decreases the oxygen mobility, and causes a slow incorporation rate of oxygen in the lattice. Cellier *et al.*<sup>136</sup> investigated the influence of the VOC nature in the total oxidation of *n*-hexane and trimethylamine over a very active  $\gamma$ -MnO<sub>2</sub> catalyst. This work shows that the extent of the catalyst reduction, which is a consequence of the Mars van Krevelen redox mechanism, depends on the nature of the organic molecule.

As previously mentioned, MnO<sub>x</sub> exhibited various structures and the tunnel-type structure has garnered considerable attention among them due to its good catalytic performance. Pyrolusite, cryptomelane and todorokite are three typical types of manganese oxide with different square tunnel sizes. Hao *et al.*<sup>137</sup> studied the influence of different tunnel structures on HCHO catalytic oxidation. MnO<sub>x</sub> with cryptomelane structure showed extremely high catalytic activity towards HCHO oxidation. It can completely oxidize HCHO at 140 °C while the temperature was increased to 180 °C and 160 °C over MnO<sub>x</sub> which have pyrolusite and todorokite structure, respectively. Characterization results revealed that the surface area, degree of crystallinity, reducibility, and average oxidation state of manganese were not the major factors governing catalytic activity towards HCHO oxidation although the tunnel structure of manganese oxide is responsible for their difference. The effective tunnel diameter of cryptomelane is close to the dynamic diameter of the HCHO molecule, which explains its high catalytic activity.

Octahedral molecular sieve (OMS-2) catalysts with different precursors and sulfate-acidified OMS-2 catalysts were synthesized using the refluxing methods.<sup>138</sup> The prepared OMS-2 catalyst with MnSO<sub>4</sub> precursor exhibited the best catalytic activity towards complete oxidation of ethanol and acetaldehyde. The Mn–O bond of OMS-2 catalysts was vital to catalytic activity toward oxidation of oxygenated VOCs. Shen *et al.*<sup>139</sup> prepared uniform manganese oxide octahedral molecular sieve (OMS-2) nanorods with cryptomelane type structure and used it for HCHO abatement. Complete conversion of HCHO can be achieved at 80 °C over OMS-2 while it was increased to 100 °C over MnO<sub>x</sub> powder under the same conditions. The results clearly demonstrate that catalytic activity is strongly related to the morphology and structure of the catalysts. Tian *et al.*<sup>140</sup> confirmed the great impact of material morphology on the catalytic performance. Two different morphologies of K-OMS-2 nanomaterials were successfully synthesized by a simple soft chemistry route. The pore channels of K-OMS-2 are favorable to the adsorption and diffusion of HCHO molecules into the inner surface of the pore channels, thus leading to a higher catalytic activity when compared with K-OMS-2 nanorods.

As the catalytic performance of MnO<sub>x</sub> is greatly affected by their structure and morphology, the synthesis of Mn-based materials with new morphologies and increased surface areas has become an attractive field.<sup>31</sup> He *et al.*<sup>141</sup> developed a facile preparation approach for monodispersed honeycomb and hollow K<sub>x</sub>MnO<sub>2</sub> nanospheres. The size and morphology of

K<sub>x</sub>MnO<sub>2</sub> nanospheres are largely dependent on the molar ratio of KMnO<sub>4</sub>/OA. Its catalytic activity was significantly higher than the previously reported MnO<sub>2</sub>, OMS-2 nanorods, MnO<sub>x</sub> powders, and Mn–Pd/Al<sub>2</sub>O<sub>3</sub> catalysts. Complete HCHO conversion can be obtained at 80 °C over hollow K<sub>x</sub>MnO<sub>2</sub> nanospheres, whereas 85 °C was required for the honeycomb nanospheres,

The effect of metal morphologies on toluene removal was also studied by Dai *et al.*<sup>129</sup> Nanosized rod-like, wire-like, and tubular  $\alpha$ -MnO<sub>2</sub> and flower-like spherical Mn<sub>2</sub>O<sub>3</sub> have been prepared *via* the hydrothermal and CCl<sub>4</sub> solution method (Fig. 8). The best catalytic activity was observed over the rod-like  $\alpha$ -MnO<sub>2</sub> catalyst. The high oxygen adspecies concentration and good low-temperature reducibility were responsible for the excellent catalytic performance.

By selectively exposing the desired facets, Fei *et al.*<sup>142</sup> prepared three distinct morphologies (*i.e.* cubic, hexagonal, and octahedral) Mn<sub>3</sub>O<sub>4</sub> nanoparticles, and revealed that catalytic activity was greatly affected by anisotropic morphologies. An apparent morphology dependence for benzene oxidation was observed with an activity sequence of (103) > (200) > (101). From the study, it seems that the well-defined morphological manganese oxides are promising materials for VOC catalytic oxidation at low temperature.

#### 4.2. Cobalt oxide

Co<sub>3</sub>O<sub>4</sub> has been known as an effective catalyst for VOC oxidation at low temperature. It has a spinel structure with a unit-cell length of 0.8084 nm. The lattice oxygen is cubic close packed in a unit cell with one-eighth of the tetrahedral sites occupied by Co<sup>2+</sup> and half of the octahedral sites occupied by Co<sup>3+</sup>.<sup>143</sup> Xie *et al.*<sup>128</sup> recently discovered that both catalytic activity and durability during CO oxidation were greatly improved as the shape of Co<sub>3</sub>O<sub>4</sub> nanoparticles was changed from spherical nanoparticles to nanorods. This is a remarkable example of the morphology effect. Recently, Li *et al.*<sup>144</sup> compared the performance of HCHO oxidation over nano-Co<sub>3</sub>O<sub>4</sub>, 2D-Co<sub>3</sub>O<sub>4</sub>, and 3D-Co<sub>3</sub>O<sub>4</sub> catalysts. The catalytic activity is in the following order: 3D-Co<sub>3</sub>O<sub>4</sub> < 2D-Co<sub>3</sub>O<sub>4</sub> < nano-Co<sub>3</sub>O<sub>4</sub>. Nano-Co<sub>3</sub>O<sub>4</sub> has a nonporous structure with low specific surface area while 2D-Co<sub>3</sub>O<sub>4</sub> and 3D-Co<sub>3</sub>O<sub>4</sub> with large specific surface areas retained the mesoporous characteristics and channel structures of the hard template. The best catalytic performance of the 3D-Co<sub>3</sub>O<sub>4</sub> catalyst is probably attributed to its rich surface active oxygen species and Co<sup>3+</sup> cationic species on the surface.

Hao *et al.*<sup>145</sup> made progress in synthesizing mesoporous Co<sub>3</sub>O<sub>4</sub> catalysts by combining the ordered mesoporous structure with exposed high activity crystal facets. High resolution transmission electron microscopy (HRTEM) studies revealed that {110} facets were exposed in the active surfaces of mesoporous Co<sub>3</sub>O<sub>4</sub>, whereas the Co<sub>3</sub>O<sub>4</sub> nanosheets prepared by the precipitation method exhibited the most exposed {112} facets, as shown in Fig. 9. The mesoporous Co<sub>3</sub>O<sub>4</sub> was significantly more active for ethylene oxidation than the Co<sub>3</sub>O<sub>4</sub>



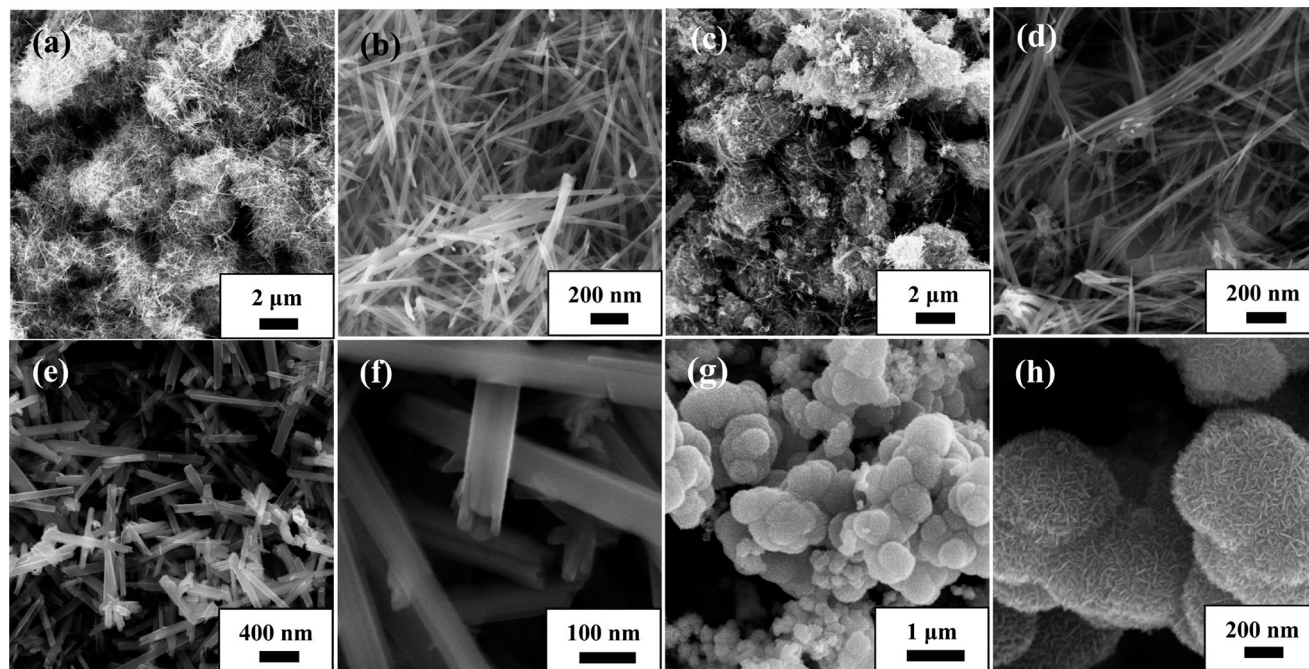


Fig. 8 SEM images of (a, b) rod-like  $\text{MnO}_2$ , (c, d) wire-like  $\text{MnO}_2$ , (e, f) tube-like  $\text{MnO}_2$ , and (g, h) flower-like  $\text{Mn}_2\text{O}_3$ .<sup>129</sup> (Reprinted with permission from F. Wang, H. Dai, J. Deng, G. Bai, K. Ji and Y. Liu, Manganese oxides with rod-, wire-, tube-, and flower-like morphologies: highly effective catalysts for the removal of toluene, *Environ. Sci. Technol.*, 2012, **46**, 4034–4041. Copyright 2012 American Chemical Society).

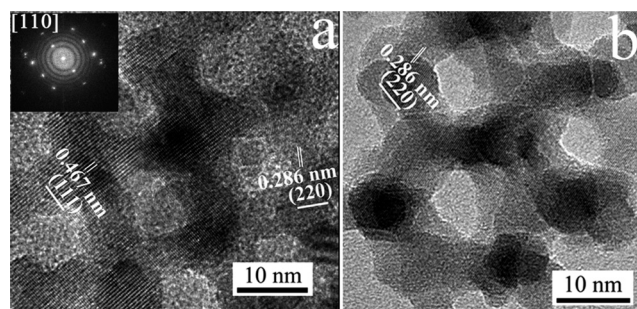


Fig. 9 HRTEM images of mesoporous  $\text{Co}_3\text{O}_4$  (a) and  $\text{Au}/\text{Co}_3\text{O}_4$  (b) prepared by the nanocasting method. The inset in panel (a) is the FFT diffractogram of the corresponding HRTEM image.<sup>145</sup> (Reprinted with permission from C. Y. Ma, Z. Mu, J. J. Li, Y. G. Jin, J. Cheng, G. Q. Lu, Z. P. Hao and S. Z. Qiao, Mesoporous  $\text{Co}_3\text{O}_4$  and  $\text{Au}/\text{Co}_3\text{O}_4$  Catalysts for Low-Temperature Oxidation of Trace Ethylene, *J. Am. Chem. Soc.*, 2010, **132**, 2608–2613. Copyright 2010, American Chemical Society).

nanosheets, indicating that the crystal facet  $\{110\}$  of  $\text{Co}_3\text{O}_4$  is crucial to its catalytic activity.

#### 4.3. Cerium oxide

Cerium is the most abundant among the rare earth elements, occupying about 0.0046 wt.% of the earth's crust. The application of cerium is increasingly spreading wide.<sup>146</sup>  $\text{CeO}_2$  has a cubic fluorite crystal structure with a cubic array of fourfold coordinated oxygen ions and cerium cations that occupy half of the eightfold coordinated cationic interstices.<sup>143</sup> It is often used as the critical component or a structural and electronic

promoter of heterogeneous catalysts for its outstanding oxygen storage capacity. Gaseous oxygen molecules can easily transfer to the surface of solid  $\text{CeO}_2$  via the quick and reversible redox between  $\text{Ce}^{4+}$  and  $\text{Ce}^{3+}$ . Furthermore, the combination of  $\text{CeO}_2$  with other oxides has been widely studied in recent years.

$\text{CeO}_2$  catalysts prepared by a thermal decomposition method were tested for the catalytic oxidation of trichloroethylene (TCE), a model of chlorinated volatile organic compounds (CVOs).<sup>147,148</sup>  $\text{CeO}_2$  catalysts exhibited a high activity for TCE catalytic combustion.  $\text{CeO}_2$  catalysts calcined at 550 °C were found to be the most effective and the  $T_{90\%}$  temperature of TCE is 205 °C (Fig. 10). The better catalytic behavior of  $\text{CeO}_2$  catalysts is attributed to surface basicity, high mobility of oxygen and oxygen-supplying ability of  $\text{CeO}_2$  catalysts.

#### 4.4. Mixed metal oxides

Mixed metal oxides were found to be highly effective for VOC oxidation by many research groups. For example, Delimaris and Ioannides<sup>149</sup> prepared  $\text{MnO}_x\text{-CeO}_2$  catalysts by a urea combustion method, in which the performance of the catalytic oxidation of ethanol, ethyl acetate and toluene was evaluated. Complete conversion of ethanol was obtained at 200 °C on  $\text{MnO}_x\text{-CeO}_2$  catalysts. It compares favorably with 0.3 wt.%  $\text{Pt}/\text{Al}_2\text{O}_3$  catalyst, on which  $T_{90\%}$  was 270 °C.<sup>150</sup> Interaction between  $\text{MnO}_x$  and  $\text{CeO}_2$  leads to structural and thermal stabilization of the catalysts and their specific surface areas are greater than those of pure  $\text{MnO}_x$  and  $\text{CeO}_2$ .



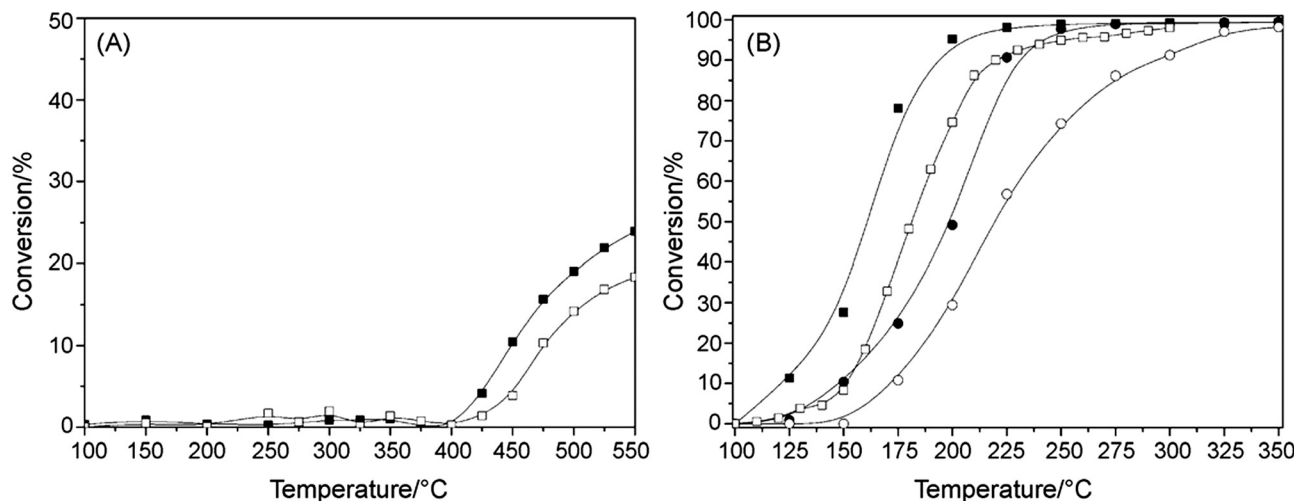


Fig. 10 TCE combustion light-off curves. Gas composition: 1000 ppm TCE, air balance; GHSV = 15 000 h<sup>-1</sup>; (A) blank test: (■) quartz; (□) none; (B) catalytic combustion over CeO<sub>2</sub> catalysts calcined at different temperatures: (■) 550 °C; (□) 450 °C; (●) 650 °C; (○) 800 °C.<sup>147</sup> (Reprinted with permission from Q. Dai, X. Wang and G. Lu, low-temperature catalytic combustion of trichloroethylene over cerium oxide and catalyst deactivation, *Appl. Catal., B*, 2008, **81**, 192–202. Copyright 2008, Elsevier).

MnO<sub>x</sub>-CeO<sub>2</sub> mixed oxides prepared by three different methods were reported by Tang *et al.*<sup>151</sup> The catalyst prepared by modified coprecipitation exhibited considerably higher catalytic activity toward complete HCHO oxidation than those prepared by sol-gel and coprecipitation methods. 100% conversion was achieved at a temperature as low as 100 °C over the former, as shown in Fig. 11. Structural analysis revealed that the high oxidation state of manganese and rich lattice oxygen species on the surface were the crucial

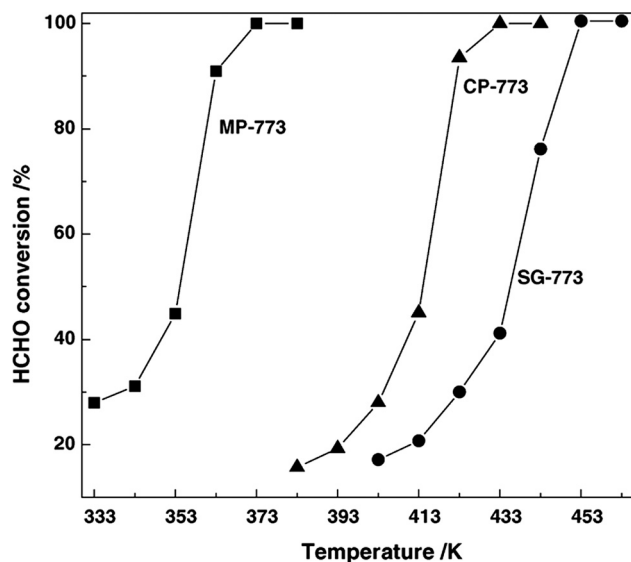


Fig. 11 Temperature dependence of HCHO conversions over the MnO<sub>x</sub>-CeO<sub>2</sub> catalysts: HCHO = 580 ppm, O<sub>2</sub> = 18.0%, He balance, GHSV = 21 000 mL g<sub>cat</sub><sup>-1</sup> h<sup>-1</sup>.<sup>151</sup> (Reprinted with permission from X. Tang, Y. Li, X. Huang, Y. Xu, H. Zhu, J. Wang and W. Shen, MnO<sub>x</sub>-CeO<sub>2</sub> mixed oxide catalysts for complete oxidation of formaldehyde: Effect of preparation method and calcination temperature, *Appl. Catal., B*, 2006, **62**, 265–273. Copyright 2006, Elsevier).

factors for the excellent catalytic performance at low temperatures. Luo *et al.*<sup>152</sup> also investigated the MnO<sub>x</sub>-CeO<sub>2</sub> mixed oxide for CO and HCHO oxidation. Although CeO<sub>2</sub> is not directly involved in the reaction, the enhanced activity was ascribed to the activation of the lattice oxygen species in MnO<sub>x</sub> by the addition of CeO<sub>2</sub>, which was confirmed by the H<sub>2</sub> temperature programmed reduction (H<sub>2</sub>-TPR).

Li *et al.*<sup>153</sup> reported a series of manganese oxides mixed with Zr, Fe, Co, and Cu oxides prepared by a reverse micro-emulsion method for catalytic oxidation of toluene. Among these metal oxides, the Cu-Mn catalyst was found to have the highest activity for complete oxidation of toluene. Mn<sub>0.67</sub>-Cu<sub>0.33</sub> (Cu loading 33 mol%) showed the total oxidation of toluene at about 220 °C, which is very close to the temperature for the reaction over Pd catalysts.<sup>73,77</sup> It was suggested that the best dispersion of the active phase may contribute significantly to the high activity of toluene oxidation over the mixed oxide catalysts.

## 5. Conclusions and outlooks

Catalytic oxidation of VOCs is highly desirable to proceed at low temperature for the consideration of energy savings, low cost, operation safety and environmental friendliness. To reduce the temperature of VOC catalytic oxidation, great efforts have been made to develop efficient catalysts, of which supported noble metal and transition metal oxides are the two successful ones. The supported noble metal exhibited superior activity toward the catalytic oxidation of VOCs at low temperature, even at room temperature for HCHO oxidation. The catalytic performance of supported noble metal is generally governed by many factors such as the properties of support and noble metal, the dispersion, size, morphology and valence of metallic particles. Therefore, numerous studies focused on how the properties of support and metal, metal

precursor, preparation and pretreatment method, reaction conditions, *etc.*, affect the properties and catalytic activity of supported noble metal catalysts during VOC oxidation. However, no clear and unified conclusions have been drawn to explain how each single parameter affects the catalytic reaction. In addition, the effect of promoters should not be ignored since they can greatly improve catalytic performance. For instance, the introduction of alkali-metal ions into Pt/TiO<sub>2</sub> catalysts stabilized an atomically dispersed Pt–O(OH)<sub>x</sub>–alkali-metal species on the catalyst surface and also opened a new low-temperature reaction pathway.<sup>58</sup> Although supported noble catalysts are the most popular and effective materials for the VOC destruction at low temperature, a considerable noble metal loading is generally required, which greatly limits its practical application due to the high cost. Hence, it is critical to reduce the noble metal loading while maintaining a high catalytic performance. Transition metal oxides are good alternatives to noble metal catalysts for the catalytic oxidation of VOCs. It has been proven that the structure and morphology of catalysts have an important influence on their catalytic activities. It has become attractive to selectively expose a larger fraction of the reactive facets on which the active sites can be enriched and tuned.<sup>143</sup> However, the mechanisms proposed for both supported noble metal and transition metal oxides are still unclear due to the limited direct and strong evidence. These greatly prevent us from understanding deeply the processes and developing highly active catalysts for VOC oxidation. More work should be carried out to study reaction mechanisms with the fast developing characterization techniques, especially *in situ* analysis instruments.

Although great achievements have been obtained in the catalytic oxidation of HCHO even at room temperature, it is still a big challenge to catalytically oxidize other VOCs at lower temperature that is even close to ambient temperature. In addition, there are still some aspects that deserve further studies in consideration of practical application. For example, the stability and durability of catalysts should be given special attention to, since the catalysts probably get deactivated more easily due to the adsorption of water vapor and intermediates on the surface at low temperature. In addition, a few studies have been carried out in terms of catalytic oxidation of mixed VOCs from industrial processes and highly diluted VOCs from indoor environments, of which the performance and mechanism are probably quite different from those of catalytic oxidation of single VOC that has high concentration. Therefore, more academic and industrial efforts must be devoted to these aspects.

## Acknowledgements

The authors gratefully acknowledge the financial support from the National Nature Science Foundation of China (no. 51208207), the Doctoral Program of Higher Education of China (no. 20120172120039), the Science and Technology

Project in Guangzhou (no. 2014Y2-00094), and the Fundamental Research Funds for the Central Universities (no. 13lgzd03).

## References

- 1 R. M. Heck and R. J. Farrauto, *Catalytic Pollution Control*, Wiley Interscience, New York, 2nd edn, 2002.
- 2 M. Amann and M. Lutz, *J. Hazard. Mater.*, 2000, **78**, 41–62.
- 3 N. Li and F. Gaillard, *Appl. Catal., B*, 2009, **88**, 152–159.
- 4 F. N. Aguero, B. P. Barbero, L. Gambaro and L. E. Cadus, *Appl. Catal., B*, 2009, **91**, 108–112.
- 5 H. L. Chen, H. M. Lee, S. H. Chen, M. B. Chang, S. J. Yu and S. N. Li, *Environ. Sci. Technol.*, 2009, **43**, 2216–2227.
- 6 R. Huang, Y. Zhang, C. Bozzetti, K. Ho, J. Cao, Y. Han, K. R. Daellenbach, J. G. Slowik, S. M. Platt, F. Canonaco, P. Zotter, R. Wolf, S. M. Pieber, E. A. Bruns, M. Crippa, G. Ciarelli, A. Piazzalunga, M. Schwikowski, G. Abbaszade, J. Schnelle-Kreis, R. Zimmermann, Z. An, S. Szidat, U. Baltensperger, I. El Haddad and A. S. H. Prevot, *Nature*, 2014, **514**, 218–222.
- 7 S. Scire and L. F. Liotta, *Appl. Catal., B*, 2012, **125**, 222–246.
- 8 J. Mo, Y. Zhang, Q. Xu, J. J. Lamson and R. Zhao, *Atmos. Environ.*, 2009, **43**, 2229–2246.
- 9 S. Morales-Torres, F. J. Maldonado-Hodar, A. F. Perez-Cadenas and F. Carrasco-Marin, *J. Hazard. Mater.*, 2010, **183**, 814–822.
- 10 R. Wang and J. Li, *Environ. Sci. Technol.*, 2010, **44**, 4282–4287.
- 11 P. Hunter and S. T. Oyama, *Control of Volatile Organic Compound Emissions*, John Wiley, New York, 2000.
- 12 E. Rivi re, *CITEPA Report*, Paris, 1998.
- 13 H. Fontane, M. Veillerot, J. C. Gallo and R. Guillermo, *Proceedings of the 8th International Symposium on Transport and Air Pollution*, Graz, 1999.
- 14 V. J. Feron, J. E. H. Arts and P. J. van Bladeren, *Pollut. Atmos.*, 1992, **134**, 18–25.
- 15 L. F. Liotta, *Appl. Catal., B*, 2010, **100**, 403–412.
- 16 L. Malhautier, G. Quijano, M. Avezac, J. Rocher and J. L. Fanlo, *Chem. Eng. J.*, 2014, **247**, 199–204.
- 17 L. Li, S. Liu and J. Liu, *J. Hazard. Mater.*, 2011, **192**, 683–690.
- 18 F. Thevenet, L. Sivachandiran, O. Guaitella, C. Barakat and A. Rousseau, *J. Phys. D: Appl. Phys.*, 2014, **47**, 224011.
- 19 H. Destailats, M. Sleiman, D. P. Sullivan, C. Jacquiod, J. Sablayrolles and L. Molins, *Appl. Catal., B*, 2012, **128**, 159–170.
- 20 O. Debono, F. Thevenet, P. Gravejat, V. Hequet, C. Raillard, L. Lecoq and N. Locoge, *Appl. Catal., B*, 2011, **106**, 600–608.
- 21 M. Yuan, C. Chang, J. Shie, C. Chang, J. Chen and W. Tsai, *J. Hazard. Mater.*, 2010, **175**, 809–815.
- 22 K. Everaert and J. Baeyens, *J. Hazard. Mater.*, 2004, **109**, 113–139.
- 23 G. R. Parmar and N. N. Rao, *Crit. Rev. Environ. Sci. Technol.*, 2008, **39**, 41–78.
- 24 J. N. Armor, *Appl. Catal., B*, 1992, **1**, 221–256.
- 25 J. J. Spivey, *Ind. Eng. Chem. Res.*, 1987, **26**, 2165–2180.

- 26 C. He, J. Li, J. Cheng, L. Li, P. Li, Z. Hao and Z. P. Xu, *Ind. Eng. Chem. Res.*, 2009, **48**, 6930–6936.
- 27 M. Luo, M. He, Y. Xie, P. Fang and L. Jin, *Appl. Catal., B*, 2007, **69**, 213–218.
- 28 L. F. Liotta, M. Ousmane, G. Di Carlo, G. Pantaleo, G. Deganello, A. Boreave and A. Giroir-Fendler, *Catal. Lett.*, 2009, **127**, 270–276.
- 29 M. Alifanti, M. Florea and V. I. Parvulescu, *Appl. Catal., B*, 2007, **70**, 400–405.
- 30 S. Morales-Torres, A. F. Perez-Cadenas, F. Kapteijn, F. Carrasco-Marin, F. J. Maldonado-Hodar and J. A. Moulijn, *Appl. Catal., B*, 2009, **89**, 411–419.
- 31 J. Q. Torres, S. Royer, J. Bellat, J. Giraudon and J. Lamonier, *ChemSusChem*, 2013, **6**, 578–592.
- 32 M. Paulis, H. Peyrard and M. Montes, *J. Catal.*, 2001, **199**, 30–40.
- 33 K. T. Chuang, B. Zhou and S. Tong, *Ind. Eng. Chem. Res.*, 1994, **33**, 1680–1686.
- 34 C. Zhang, H. He and K. Tanaka, *Catal. Commun.*, 2005, **6**, 211–214.
- 35 H. Huang and D. Y. C. Leung, *J. Catal.*, 2011, **280**, 60–67.
- 36 M. Stoyanova, P. Konova, P. Nikolov, A. Naydenov, S. Christoskova and D. Mehandjiev, *Chem. Eng. J.*, 2006, **122**, 41–46.
- 37 M. A. Alvarez-Merino, M. F. Ribeiro, J. M. Silva, F. Carrasco-Marin and F. J. Maldonado-Hodar, *Environ. Sci. Technol.*, 2004, **38**, 4664–4670.
- 38 R. K. Grasselli, *Top. Catal.*, 2002, **21**, 79–88.
- 39 S. Balasubramanian and D. S. Viswanath, *Ind. Eng. Chem. Fundam.*, 1975, **14**, 158–165.
- 40 H. L. Tidahy, M. Hosseini, S. Siffert, R. Cousin, J. F. Lamonier, A. Aboukais, B. L. Su, J. M. Giraudon and G. Leclercq, *Catal. Today*, 2008, **137**, 335–339.
- 41 S. Ordó Ez, L. Bello, H. Sastre, R. Rosal and F. V. Díez, *Appl. Catal., B*, 2002, **38**, 139–149.
- 42 Y. Yazawa, N. Takagi, H. Yoshida, S. Komai, A. Satsuma, T. Tanaka, S. Yoshida and T. Hattori, *Appl. Catal., A*, 2002, **233**, 103–112.
- 43 H. Huang, P. Hu, H. Huang, J. Chen, X. Ye and D. Y. C. Leung, *Chem. Eng. J.*, 2014, **252**, 320–326.
- 44 K. Kim and H. Ahn, *Appl. Catal., B*, 2009, **91**, 308–318.
- 45 T. F. Garetto and C. R. Apesteguia, *Appl. Catal., B*, 2001, **32**, 83–94.
- 46 T. Barakat, J. C. Rooke, H. L. Tidahy, M. Hosseini, R. Cousin, J. Lamonier, J. Giraudon, G. De Weireld, B. Su and S. Siffert, *ChemSusChem*, 2011, **4**, 1420–1430.
- 47 S. Scirè, S. Minicò and C. Crisafulli, *Appl. Catal., B*, 2003, **45**, 117–125.
- 48 Q. H. Xia, K. Hidajat and S. Kawi, *Catal. Today*, 2001, **68**, 255–262.
- 49 J. Chi-Sheng Wu and T. Chang, *Catal. Today*, 1998, **44**, 111–118.
- 50 V. Gaur, A. Sharma and N. Verma, *Carbon*, 2005, **43**, 3041–3053.
- 51 T. Masui, H. Imadzu, N. Matsuyama and N. Imanaka, *J. Hazard. Mater.*, 2010, **176**, 1106–1109.
- 52 N. Imanaka, T. Masui, K. Koyabu, K. Minami and T. Egawa, *Adv. Mater.*, 2007, **19**, 1608.
- 53 C. Zhang and H. He, *Catal. Today*, 2007, **126**, 345–350.
- 54 C. Zhang, H. He and K. Tanaka, *Appl. Catal., B*, 2006, **65**, 37–43.
- 55 J. Peng and S. Wang, *Appl. Catal., B*, 2007, **73**, 282–291.
- 56 L. Nie, Y. Zheng and J. Yu, *Dalton Trans.*, 2014, **43**, 12935–12942.
- 57 H. Huang, D. Y. C. Leung and D. Ye, *J. Mater. Chem.*, 2011, **21**, 9647.
- 58 C. Zhang, F. Liu, Y. Zhai, H. Ariga, N. Yi, Y. Liu, K. Asakura, M. Flytzani-Stephanopoulos and H. He, *Angew. Chem., Int. Ed.*, 2012, **51**, 9628–9632.
- 59 L. Nie, J. Yu, X. Li, B. Cheng, G. Liu and M. Jaroniec, *Environ. Sci. Technol.*, 2013, **47**, 2777–2783.
- 60 N. An, Q. Yu, G. Liu, S. Li, M. Jia and W. Zhang, *J. Hazard. Mater.*, 2011, **186**, 1392–1397.
- 61 N. An, P. Wu, S. Li, M. Jia and W. Zhang, *Appl. Surf. Sci.*, 2013, **285**, 805–809.
- 62 X. Yu, J. He, D. Wang, Y. Hu, H. Tian and Z. He, *J. Phys. Chem. C*, 2012, **116**, 851–860.
- 63 X. Tang, J. Chen, X. Huang, Y. Xu and W. Shen, *Appl. Catal., B*, 2008, **81**, 115–121.
- 64 P. Papaefthimiou, T. Ioannides and X. E. Verykios, *Appl. Catal., B*, 1997, **13**, 175–184.
- 65 G. T. Veser, M. Ziauddin and L. D. Schmidt, *Catal. Today*, 1999, **47**, 219–228.
- 66 R. Burch, D. J. Crittle and M. J. Hayes, *Catal. Today*, 1999, **47**, 229–234.
- 67 M. Aryafar and F. Zaera, *Catal. Lett.*, 1997, **48**, 173–183.
- 68 M. Paulis, L. M. Gandia, A. Gil, J. Sambeth, J. A. Odriozola and M. Montes, *Appl. Catal., B*, 2000, **26**, 37–46.
- 69 J. C. Summers and D. R. Monroe, *Ind. Eng. Chem. Res.*, 1981, **20**, 23–31.
- 70 S. Huang, C. Zhang and H. He, *Catal. Today*, 2008, **139**, 15–23.
- 71 G. Centi, *J. Mol. Catal. A: Chem.*, 2001, **173**, 287–312.
- 72 M. C. Álvarez-Galván, B. Pawelec, V. A. de la Peña O Shea, J. L. G. Fierro and P. L. Arias, *Appl. Catal., B*, 2004, **51**, 83–91.
- 73 K. Okumura, T. Kobayashi, H. Tanaka and M. Niwa, *Appl. Catal., B*, 2003, **44**, 325–331.
- 74 P. Li, C. He, J. Cheng, C. Y. Ma, B. J. Dou and Z. P. Hao, *Appl. Catal., B*, 2011, **101**, 570–579.
- 75 H. L. Tidahy, S. Siffert, J. F. Lamonier, R. Cousin, E. A. Zhilinskaya, A. Aboukais, B. L. Su, X. Canet, G. De Weireld, M. Frère, J. M. Giraudon and G. Leclercq, *Appl. Catal., B*, 2007, **70**, 377–383.
- 76 H. L. Tidahy, S. Siffert, F. Wyrwalski, J. F. Lamonier and A. Aboukais, *Catal. Today*, 2007, **119**, 317–320.
- 77 H. L. Tidahy, S. Siffert, J. F. Lamonier, E. A. Zhilinskaya, A. Aboukais, Z. Y. Yuan, A. Vantomme, B. L. Su, X. Canet, G. De Weireld, M. Frère, T. B. N. Guyen, J. M. Giraudon and G. Leclercq, *Appl. Catal., A*, 2006, **310**, 61–69.
- 78 S. C. Kim and W. G. Shim, *Appl. Catal., B*, 2009, **92**, 429–436.

- 79 S. Ihm, Y. Jun, D. Kim and K. Jeong, *Catal. Today*, 2004, **93–95**, 149–154.
- 80 W. G. Shim, J. W. Lee and S. C. Kim, *Appl. Catal., B*, 2008, **84**, 133–141.
- 81 S. C. Su, J. N. Carstens and A. T. Bell, *J. Catal.*, 1998, **176**, 125–135.
- 82 R. J. Farrauto, J. K. Lampert, M. C. Hobson and E. M. Waterman, *Appl. Catal., B*, 1995, **6**, 263–270.
- 83 P. O. Thevenin, A. Alcalde, L. J. Pettersson, S. G. Järås and J. L. G. Fierro, *J. Catal.*, 2003, **215**, 78–86.
- 84 H. Huang and D. Y. C. Leung, *ACS Catal.*, 2011, **1**, 348–354.
- 85 H. Huang, X. Ye, H. Huang, L. Zhang and D. Y. C. Leung, *Chem. Eng. J.*, 2013, **230**, 73–79.
- 86 C. Zhang, Y. Li, Y. Wang and H. He, *Environ. Sci. Technol.*, 2014, **48**, 5816–5822.
- 87 M. Haruta, N. Yamada, T. Kobayashi and S. Iijima, *J. Catal.*, 1989, **115**, 301–309.
- 88 R. D. Waters, J. J. Weimer and J. E. Smith, *Catal. Lett.*, 1994, **30**, 181–188.
- 89 M. Haruta, A. Ueda, S. Tsubota and R. M. Torres Sanchez, *Catal. Today*, 1996, **29**, 443–447.
- 90 B. Chen, C. Bai, R. Cook, J. Wright and C. Wang, *Catal. Today*, 1996, **30**, 15–20.
- 91 M. Haruta, *Catal. Today*, 1997, **36**, 153–166.
- 92 M. Haruta, S. Tsubota, T. Kobayashi, H. Kageyama, M. J. Genet and B. Delmon, *J. Catal.*, 1993, **144**, 175–192.
- 93 G. C. Bond and D. T. Thompson, *Catal. Rev.: Sci. Eng.*, 1999, **41**, 319–388.
- 94 S. Minico, S. Scire, C. Crisafulli, R. Maggiore and S. Galvagno, *Appl. Catal., B*, 2000, **28**, 245–251.
- 95 J. Qi, J. Chen, G. Li, S. Li, Y. Gao and Z. Tang, *Energy Environ. Sci.*, 2012, **5**, 8937–8941.
- 96 S. Scirè, S. Minicò, C. Crisafulli and S. Galvagno, *Catal. Commun.*, 2001, **2**, 229–232.
- 97 R. J. H. Grisel, P. J. Kooyman and B. E. Nieuwenhuys, *J. Catal.*, 2000, **191**, 430–437.
- 98 R. Grisel and B. E. Nieuwenhuys, *Catal. Today*, 2001, **64**, 69–81.
- 99 C. Cellier, S. Lambert, E. M. Gaigneaux, C. Poleunis, V. Ruaux, P. Eloy, C. Lahousse, P. Bertrand, J. P. Pirard and P. Grange, *Appl. Catal., B*, 2007, **70**, 406–416.
- 100 S. Minicò, S. Scirè, C. Crisafulli and S. Galvagno, *Appl. Catal., B*, 2001, **34**, 277–285.
- 101 B. E. Solsona, T. Garcia, C. Jones, S. H. Taylor, A. F. Carley and G. J. Hutchings, *Appl. Catal., A*, 2006, **312**, 67–76.
- 102 B. Solsona, E. Aylon, R. Murillo, A. M. Mastral, A. Monzonis, S. Agouram, T. E. Davies, S. H. Taylor and T. Garcia, *J. Hazard. Mater.*, 2011, **187**, 544–552.
- 103 M. A. Centeno, M. Paulis, M. Montes and J. A. Odriozola, *Appl. Catal., A*, 2002, **234**, 65–78.
- 104 S. Scirè, S. Minicò, C. Crisafulli, C. Satriano and A. Pistone, *Appl. Catal., B*, 2003, **40**, 43–49.
- 105 M. Ousmane, L. F. Liotta, G. Di Carlo, G. Pantaleo, A. M. Venezia, G. Deganello, L. Retailleau, A. Boreave and A. Giroir-Fendler, *Appl. Catal., B*, 2011, **101**, 629–637.
- 106 B. Chen, C. Shi, M. Crocker, Y. Wang and A. Zhu, *Appl. Catal., B*, 2013, **132**, 245–255.
- 107 M. Jia, Y. Shen, C. Li, Z. Bao and S. Sheng, *Catal. Lett.*, 2005, **99**, 235–239.
- 108 Y. Shen, X. Yang, Y. Wang, Y. Zhang, H. Zhu, L. Gao and M. Jia, *Appl. Catal., B*, 2008, **79**, 142–148.
- 109 H. Li, N. Zhang, P. Chen, M. Luo and J. Lu, *Appl. Catal., B*, 2011, **110**, 279–285.
- 110 C. Li, Y. Shen, M. Jia, S. Sheng, M. O. Adebajo and H. Zhu, *Catal. Commun.*, 2008, **9**, 355–361.
- 111 B. Chen, X. Zhu, M. Crocker, Y. Wang and C. Shi, *Appl. Catal., B*, 2014, **154**, 73–81.
- 112 Y. Zhang, Y. Shen, X. Yang, S. Sheng, T. Wang, M. F. Adebajo and H. Zhu, *J. Mol. Catal. A: Chem.*, 2010, **316**, 100–105.
- 113 B. Liu, Y. Liu, C. Li, W. Hu, P. Jing, Q. Wang and J. Zhang, *Appl. Catal., B*, 2012, **127**, 47–58.
- 114 J. Zhang, Y. Jin, C. Li, Y. Shen, L. Han, Z. Hu, X. Di and Z. Liu, *Appl. Catal., B*, 2009, **91**, 11–20.
- 115 B. Liu, C. Li, Y. Zhang, Y. Liu, W. Hu, Q. Wang, L. Han and J. Zhang, *Appl. Catal., B*, 2012, **111–112**, 467–475.
- 116 B. R. Cuenya, *Thin Solid Films*, 2010, **518**, 3127–3150.
- 117 Y. Liu, H. Dai, J. Deng, S. Xie, H. Yang, W. Tan, W. Han, Y. Jiang and G. Guo, *J. Catal.*, 2014, **309**, 408–418.
- 118 M. Hosseini, T. Barakat, R. Cousin, A. Aboukais, B. L. Su, G. De Weireld and S. Siffert, *Appl. Catal., B*, 2012, **111–112**, 218–224.
- 119 C. Y. Ma, B. J. Dou, J. J. Li, J. Cheng, Q. Hu, Z. P. Hao and S. Z. Qiao, *Appl. Catal., B*, 2009, **92**, 202–208.
- 120 A. Wang, X. Y. Liu, C. Mou and T. Zhang, *J. Catal.*, 2013, **308**, 258–271.
- 121 S. Imamura, D. Uchihori, K. Utani and T. Ito, *Catal. Lett.*, 1994, **24**, 377–384.
- 122 C. F. Mao and M. A. Vannice, *J. Catal.*, 1995, **154**, 230–244.
- 123 D. Chen, Z. Qu, W. Zhang, X. Li, Q. Zhao and Y. Shi, *Colloids Surf., A*, 2011, **379**, 136–142.
- 124 Z. Qu, S. Shen, D. Chen and Y. Wang, *J. Mol. Catal. A: Chem.*, 2012, **356**, 171–177.
- 125 X. Tang, J. Chen, Y. Li, Y. Li, Y. Xu and W. Shen, *Chem. Eng. J.*, 2006, **118**, 119–125.
- 126 B. Bai and J. Li, *ACS Catal.*, 2014, **4**, 2753–2762.
- 127 Z. Huang, X. Gu, Q. Cao, P. Hu, J. Hao, J. Li and X. Tang, *Angew. Chem.*, 2012, **124**, 4274–4279.
- 128 X. Xie, Y. Li, Z. Liu, M. Haruta and W. Shen, *Nature*, 2009, **458**, 746–749.
- 129 F. Wang, H. Dai, J. Deng, G. Bai, K. Ji and Y. Liu, *Environ. Sci. Technol.*, 2012, **46**, 4034–4041.
- 130 Y. Wei, J. Liu, Z. Zhao, A. Duan, G. Jiang, C. Xu, J. Gao, H. He and X. Wang, *Energy Environ. Sci.*, 2011, **4**, 2959–2970.
- 131 Y. Sekine and A. Nishimura, *Atmos. Environ.*, 2001, **35**, 2001–2007.
- 132 Y. Sekine, *Atmos. Environ.*, 2002, **36**, 5543–5547.
- 133 Y. Chang and J. G. McCarty, *Catal. Today*, 1996, **30**, 163–170.
- 134 S. C. Kim and W. G. Shim, *Appl. Catal., B*, 2010, **98**, 180–185.



- 135 V. P. Santos, M. F. R. Pereira, J. J. M. Orfao and J. L. Figueiredo, *Appl. Catal., B*, 2010, **99**, 353–363.
- 136 C. Cellier, V. Ruaux, C. Lahousse, P. Grange and E. M. Gaigneaux, *Catal. Today*, 2006, **117**, 350–355.
- 137 T. Chen, H. Dou, X. Li, X. Tang, J. Li and J. Hao, *Microporous Mesoporous Mater.*, 2009, **122**, 270–274.
- 138 R. Wang and J. Li, *Environ. Sci. Technol.*, 2010, **44**, 4282–4287.
- 139 X. Tang, X. Huang, J. Shao, J. Liu, Y. Li, Y. Xu and W. Shen, *Chin. J. Catal.*, 2006, **27**, 97–99.
- 140 H. Tian, J. He, X. Zhang, L. Zhou and D. Wang, *Microporous Mesoporous Mater.*, 2011, **138**, 118–122.
- 141 H. Chen, J. He, C. Zhang and H. He, *J. Phys. Chem. C*, 2007, **111**, 18033–18038.
- 142 Z. Fei, B. Sun, L. Zhao, W. Ji and C. Au, *Chem. – Eur. J.*, 2013, **19**, 6480–6487.
- 143 Y. Li and W. Shen, *Chem. Soc. Rev.*, 2014, **43**, 1543–1574.
- 144 B. Bai, H. Arandiyana and J. Li, *Appl. Catal., B*, 2013, **142–143**, 677–683.
- 145 C. Y. Ma, Z. Mu, J. J. Li, Y. G. Jin, J. Cheng, G. Q. Lu, Z. P. Hao and S. Z. Qiao, *J. Am. Chem. Soc.*, 2010, **132**, 2608–2613.
- 146 M. A. K. M. Hanafiah, Z. M. Hussin, N. F. M. Ariff, W. S. W. Ngah and S. C. Ibrahim, *Adv. Mater. Res.*, 2014, **970**, 198–203.
- 147 Q. Dai, X. Wang and G. Lu, *Appl. Catal., B*, 2008, **81**, 192–202.
- 148 Q. Dai, X. Wang and G. Lu, *Catal. Commun.*, 2007, **8**, 1645–1649.
- 149 D. Delimaris and T. Ioannides, *Appl. Catal., B*, 2008, **84**, 303–312.
- 150 G. Avgouropoulos, E. Oikonomopoulos, D. Kanistras and T. Ioannides, *Appl. Catal., B*, 2006, **65**, 62–69.
- 151 X. Tang, Y. Li, X. Huang, Y. Xu, H. Zhu, J. Wang and W. Shen, *Appl. Catal., B*, 2006, **62**, 265–273.
- 152 X. Liu, J. Lu, K. Qian, W. Huang and M. Luo, *J. Rare Earths*, 2009, **27**, 418–424.
- 153 W. B. Li, W. B. Chu, M. Zhuang and J. Hua, *Catal. Today*, 2004, **93–95**, 205–209.